ANALYSIS OF ELECTROMAGNETIC LAUNCHER DESIGN AND MODELING

A Thesis

presented to

the Faculty of California Polytechnic State University,

San Luis Obispo

In Partial Fulfillment

of the Requirements for the Degree

Master of Science in Electrical Engineering

by

Garrett Ross Germany

June 2016

COMMITTEE MEMBERSHIP

TITLE:	Analysis of Electromagnetic Launcher Design and Modeling
AUTHOR:	Garrett Ross Germany
DATE SUBMITTED:	June 2016
COMMITTEE CHAIR:	Vladimir Prodanov, Ph.D. Associate Professor of Electrical Engineering
COMMITTEE MEMBER:	Kira Abercromby, Ph.D. Associate Professor of Aeronautics
COMMITTEE MEMBER:	Taufik, Ph.D. Professor of Electrical Engineering

ABSTRACT

Analysis of Electromagnetic Launcher Design and Modeling

Garrett Ross Germany

This thesis derives working expressions from electromagnetic physical laws to gain a deeper understanding of the nature of railguns. The expressions are refined for ease of use and then compared to electromagnetic simulators that solve complex equations that arise from different rail geometry. Further simplifications lead to an expression for the final velocity of the projectile and showcase the importance of the system resistance to projectile flux gain ratio. A Simulink simulation then incorporates the resulting non-linear differential equations and approximates the projectile velocity over time based on physical dimensions and material properties. Some equations derived can be found in literature regarding the subject but often lack explanation. This work is intended to provide a thorough derivation of all the relative constituent relations between the critical characteristics of the gun such as the strength of the forces acting on the rail and projectile, rail current, and initial velocity of the projectile. This makes it easier to identify what influences acceleration of the projectile, how much bracing each rail needs, how much initial velocity to give the projectile, etc. Design options discussed besides the standard design include the augmented rail system, a magnetic shell design, and a “wrap around” design. The tradeoffs encountered in each design are discussed in length. Due to the lack of a sufficient power source during testing the projectile was unable to travel down the

length of the rails due to metal binding, insufficient pulse duration, and too much circuit resistance. It was found that using copper tungsten for the rails ensures that the rails can withstand the arcing inflicted by the kilo-Ampere current along the rails very well compared to other materials. Also, the copper in the tungsten alloy ensures high conductivity while the tungsten provides structural integrity to the rails during arcing between them and the projectile. Frequency response of conductive projectiles is characterized and improvements such as laminated projectiles are suggested as solutions to mitigate eddy currents induced in the projectile and improve performance.

ACKNOWLEDGMENTS

I'd like to thank my advisor Prodanov for supplying the capacitors that were used in this project. I would also like to thank Sam Jaffe for lending me his equipment to conduct tests and acquire data from them. Without either of their help the project likely wouldn't have gotten as far as it did. I would also like to thank my committee members for taking time out of their busy schedules to attend my defense.

TABLE OF CONTENTS

LIST OF TABLES

LIST OF FIGURES

1 Introduction

On February 2012 the US Navy demonstrated a 32 MJ railgun successfully firing a metal sabot between Mach 6 & 7 [1]. The device is projected to have a range of 100 nautical miles and a very short time to impact compared to conventional weapons [2]. The munitions themselves are not explosive leading to safe munitions storage and reducing the risk of explosion aboard a ship. Since then the Navy has been making terrific strides to reduce size, increase rate of fire, and extend rail lifetime of the railgun. Currently the Navy is funding a 64 MJ prototype as part of a phase II of a larger program. Even if all of the goals aren't achieved, the project has the potential transform naval warfare so much that old strategies may need to change or become outdated. Now more than ever it seems that railguns may become common place among military and scientific organizations as improvement continues and old records are repeatedly being broken.

Traditionally there haven't been many options available for applications that need a projectile with any significant mass to be greatly accelerated through a barrel in a short time. Usually light gas guns (LGG) achieve the best results per material cost and are commonly used in physics experiments that require the acceleration. Some of these experiments, for example, deal with space debris shield testing. Since space debris is known to slam into satellites up to speeds of 3km/s researchers need a device that can accelerate a projectile with a mass on the order of grams to orbital speeds before ejecting the projectile towards the shield.

The concept of a railgun has existed for nearly a 100 years with one of the first US patents being issued to Fauchon Villeplee in 1919 [3]. However, not much development occurred during this time due to the expense involved in building the necessary electrical components to power such a device, and material required for rail construction that could withstand tremendous arcing while possessing good electrical conductivity. As technology has progressed many of these restrictions aren't nearly as daunting as they were back then such that now governments and scientists are re-evaluating their feasibility. The best way to accomplish such a task is to develop an accurate model of the railgun as a whole along with a thorough understanding.

2 Analysis

We begin by identifying the central principle behind the operation of a railgun - the Lorentz force. It states that the force due to a current, enclosed in a magnetic field, is given by the equation [4]:

$$\vec{F} = I\vec{L} \times \vec{B} \qquad \text{Equation 1}$$

That is the force vector $\vec{F}$ is equal to the cross product of the vector $I\vec{L}$ (whose magnitude is equal to length of the conductor scaled by the current), and flux density vector $\vec{B}$ present on the conductor.

According to Lenz's law we can use right hand rule to identify the direction of the B field (B is technically a vector field that assigns a vector to every point in space) due to current by pointing our right hand thumb in the direction of the current, and curling our fingers towards the palm of our hand as shown below in Figure 1 [5].

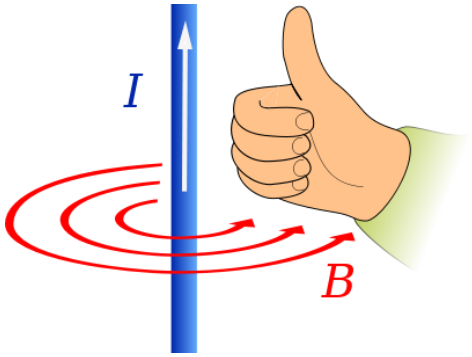

Figure 1: How to Interpret Right Hand Rule

If we select a point in space and want to know the direction of $\vec{B}$ we can picture the point as lying on a circle centered and perpendicular about the wire as seen in Figure 1 (with 3 circles) with a direction that is tangent to the circle. We know the direction of the B field in space but we are still missing the magnitude. Biot-Savart's law is required and is often stated in the following matter in Figure 2.

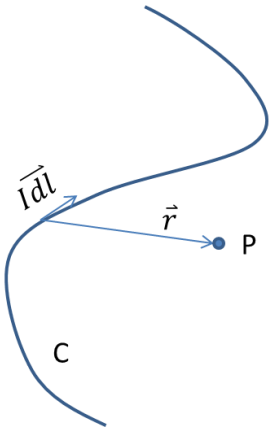

$$\vec{B}(P) = \frac{\mu_0}{4\pi}\int \frac{\vec{Idl} \times \vec{r}}{|\vec{r}|^3}$$

Equation 2

Figure 2: Biot-Savart's Law Illustrated

Where $\vec{r} = r - l$ (r being the position vector along the circle and l being the position vector of a point on the conductor), $\vec{Idl}$ is a vector whose magnitude is scaled by the current and direction is tangent to the direction of the conductor, and μ_0 is the permeability of free space [6].

2.1 Describing Rail Flux Density

We are now able to analyze the magnetic field of a single rail with finite length. To simplify things, we will assume that the rail has no volume and is nothing more than a line that exists in 3D space. Later we'll show the error introduced by this assumption is negligible under most circumstances and can be applied to both round and square rails.

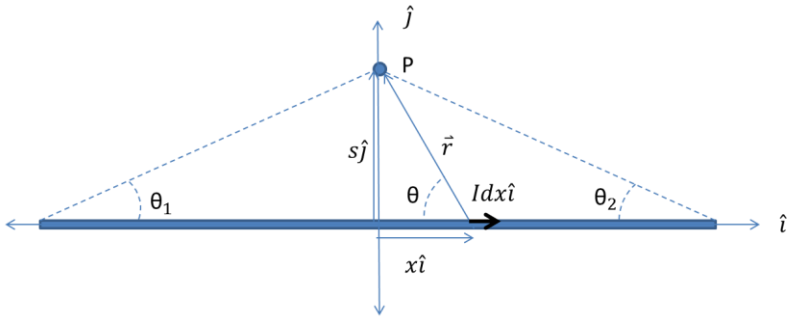

Figure 3: Flux Density of Finite Length, Current Carrying, Zero-Volume Conductor

Figure 3 illustrates the mathematical framework and variable definitions we'll be using (the unit vector $\hat{k}$ is coming out of the page). To use Biot-Savart's law we must develop an expression for $I\overrightarrow{dl} \times \vec{r}$. First we note:

$$\vec{r} = [\sin(\theta)\,\hat{\jmath} - \cos(\theta)\,\hat{\imath}]\sqrt{s^2 + x^2} \qquad \text{Equation 3}$$

$$I\overrightarrow{dl} = Idx\hat{\imath} \qquad \text{Equation 4}$$

Thus:

$$I\overrightarrow{dl} \times \vec{r} = Idx\hat{\imath} \times [\sin(\theta)\,\hat{\jmath} - \cos(\theta)\,\hat{\imath}]\sqrt{s^2 + x^2} \qquad \text{Equation 5}$$

$$I\overrightarrow{dl} \times \vec{r} = I\sin(\theta)\sqrt{s^2 + x^2}\,dx\hat{k} \qquad \text{Equation 6}$$

We substitute the original variables for what we know to get a full expression for: $\frac{I\overrightarrow{dl}\times\vec{r}}{|\vec{r}|^3}$

$$\frac{I\overrightarrow{dl}\times\vec{r}}{|\vec{r}|^3} = \frac{Isin(\theta)}{|\vec{r}|^2}dx\hat{k} \qquad \text{Equation 7}$$

However the bounds of the integral are angles. Therefore we want terms $|\vec{r}|$ and x as an expression of θ and then substitute that in for those variables. [7] Notice:

$$|\vec{r}| = s[csc(\theta)] \qquad \text{Equation 8}$$

$$x = \mathrm{s}[\cot(\theta)] \;\rightarrow dx = -s[csc^2(\theta)]d\theta \qquad \text{Equation 9}$$

$$\frac{I\overrightarrow{dl}\times\vec{r}}{|\vec{r}|^3} = \frac{Isin(\theta)}{|\vec{r}|^2} = \frac{-s[csc^2(\theta)]I\sin(\theta)d\theta\hat{k}}{s^2csc^2(\theta)} = \frac{-Isin(\theta)d\theta\hat{k}}{s} \qquad \text{Equation 10}$$

Now the integral becomes:

$$B(P) = \frac{\mu_0 I}{4\pi}\int_{\pi-\theta_1}^{\theta_2}\frac{-sin(\theta)}{s}d\theta\hat{k} \qquad \text{Equation 11}$$

The lower bound of the integral is such because θ_1 is measured from a different reference than variable θ. The expression: π-θ_1, finds the angle measured from the proper reference. Integrating we find:

$$B(P) = \frac{\mu_0 I}{4\pi}\frac{cos(\theta)}{s}\hat{k}\Big|_{\pi-\theta_1}^{\theta_2} \quad \text{Equation 12}$$

$$B(P) = \frac{\mu_0 I}{4\pi s}[cos(\theta_2) - \cos(\pi - \theta_1)]\hat{k} \quad \text{Equation 13}$$

$$\boldsymbol{B(P) = \frac{\mu_0 I}{4\pi s}[\cos(\theta_1) + cos(\theta_2)]} \quad \text{Equation 14}$$

We can drop the unit vector $\hat{k}$ and just use right hand rule. Equation 14 above is very fundamental. It gives us the strength of the B field due to a finite length conducting rail at any given point in space outside the conductor. Combined with right hand rule, we have a complete description of the B field for straight rails.

2.2 Approximating Effects Due to Rail Shape

We examine just how good of an approximation Equation 14 is for the B field outside various non-zero volume conductors. We want to know if the expression above works well for other rail geometries besides cylindrical such as square or rectangular rails. Solving such expressions is often very difficult and the results they yield are often hard to understand. For these questions we turn to simulation programs such as Finite Element Method Magnetics (FEMM) that implement finite element analysis techniques to approximate such answers [13]. We will be looking at cylindrical, rectangular, and square rail geometries and how or if certain aspects of their magnetic field deviate from Equation 14 as we vary the physical dimensions of the rails.

For ease of comparison all rail simulations set the rail current to 20kA and have the same cross sectional area of 4cm^2. The B field that is being measured is normal to a horizontal line that begins at the surface of the conductor, extends outward from the conductor, and whose y coordinate is the same as the conductor's center of mass. The results of the simulation of a one

meter long, 11.3mm radius cylindrical rail are shown in Figure 4. The B field is normal to the red line is plotted further down in Figure 5.

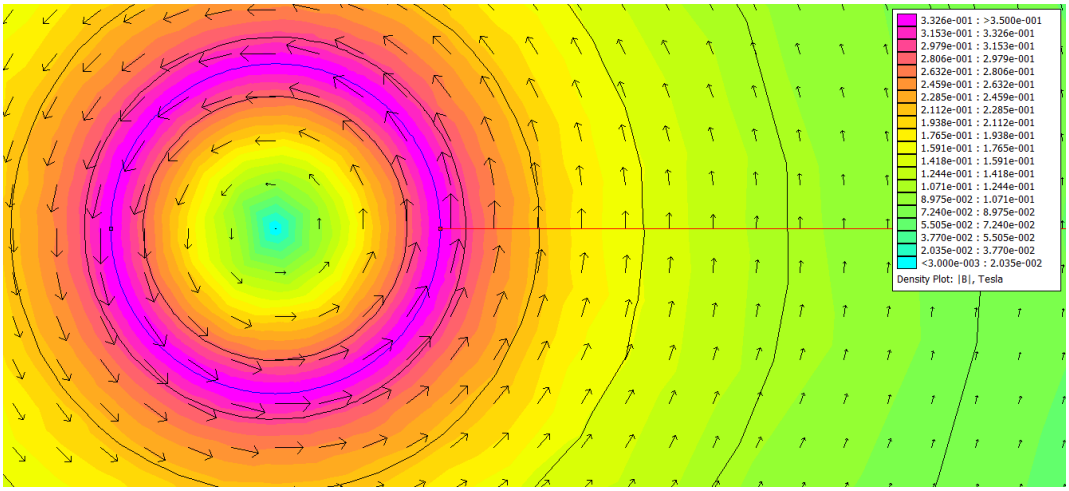

Figure 4: B Field Generated by a Cylindrical Rail Carrying 20kA

If we invoke our approximation when $\theta_1 = \theta_2 \approx 0$ and plot the magnitude of B as a function of distance from the center of the conductor, and compare that to our simulation we see that our approximation and simulation are nearly identical with an average error of .621% as long as θ_1 and $\theta_2$are close to zero.

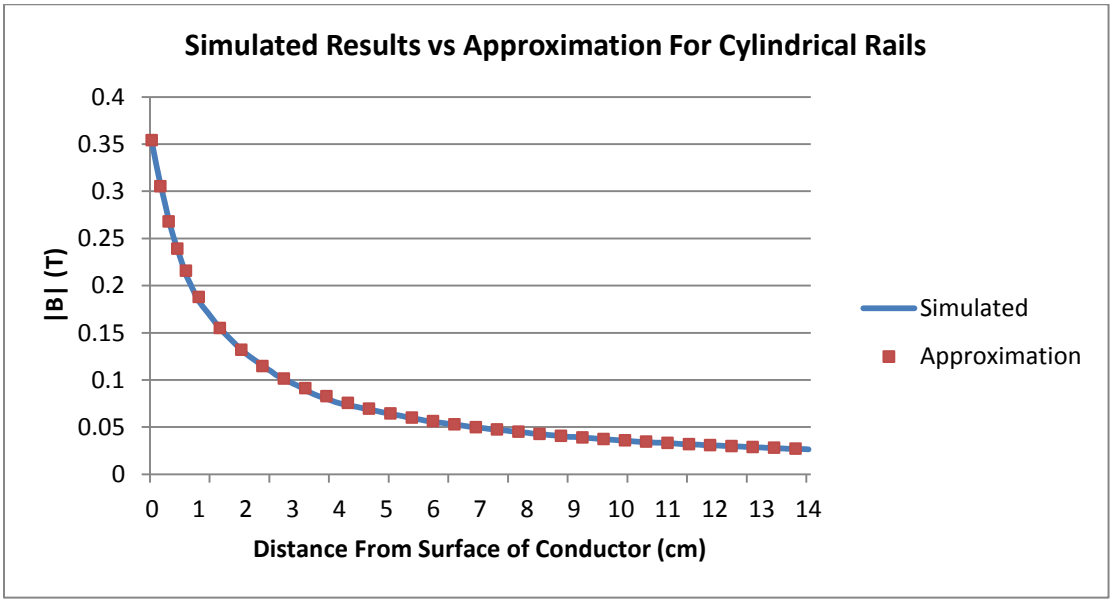

Figure 5: Comparison of Cylindrical Approximation to Simulation

As expected the approximation is nearly exact when predicting the B field of cylindrical rails, but how do the other geometries fare?

Let's look at the square rail geometry. The results below in Figure 6 are for a 1m long square rail with a side length of 2cm.

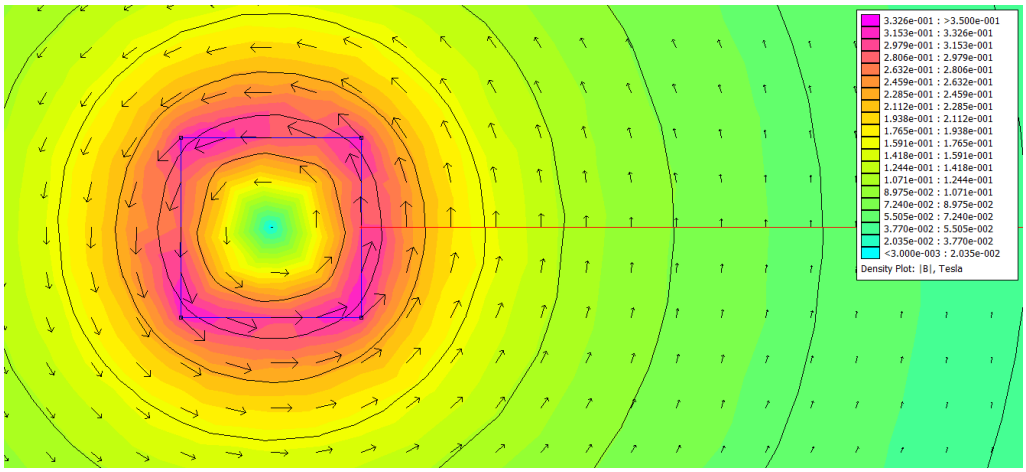

Figure 6: B Field Generated by a Square Rail Carrying 20kA

We do the same kind of plots and compare them as shown in Figure 7.

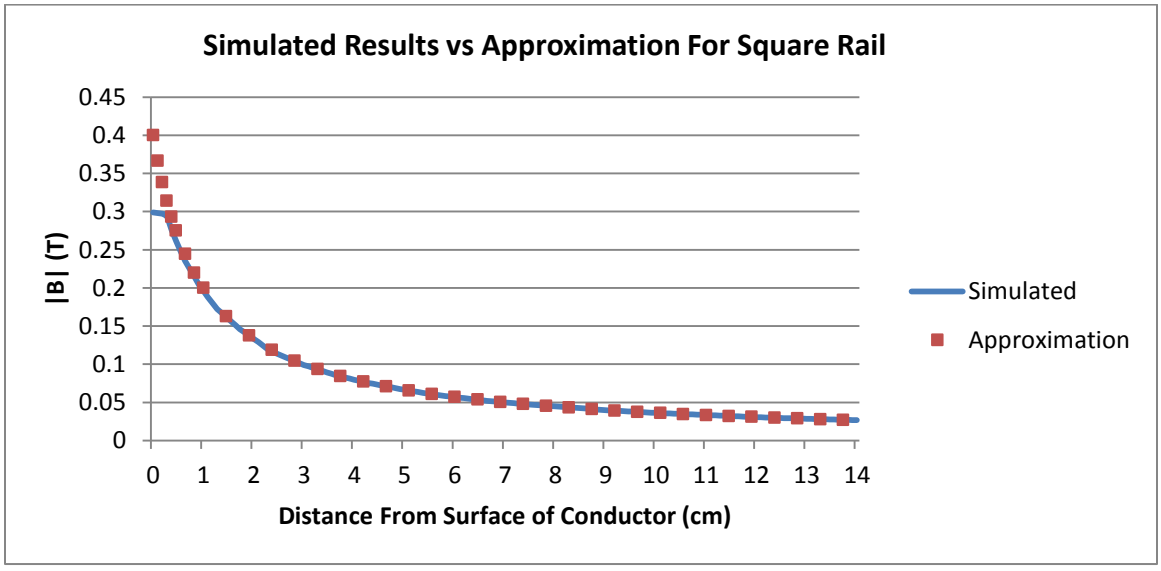

Figure 7: Comparison of Square B field vs Approximate B field

We see that the field just outside of the conductor is different from our approximation for the magnetic field near the conductor. Luckily this still remains a good approximation for the most

part as long as the projectile is wide since we integrate the perpendicular B field along this contour to find projectile force. The average error is 1.06%.

Now we examine rectangular rails. The simulation results below is for a 4x1 rectangular rail.

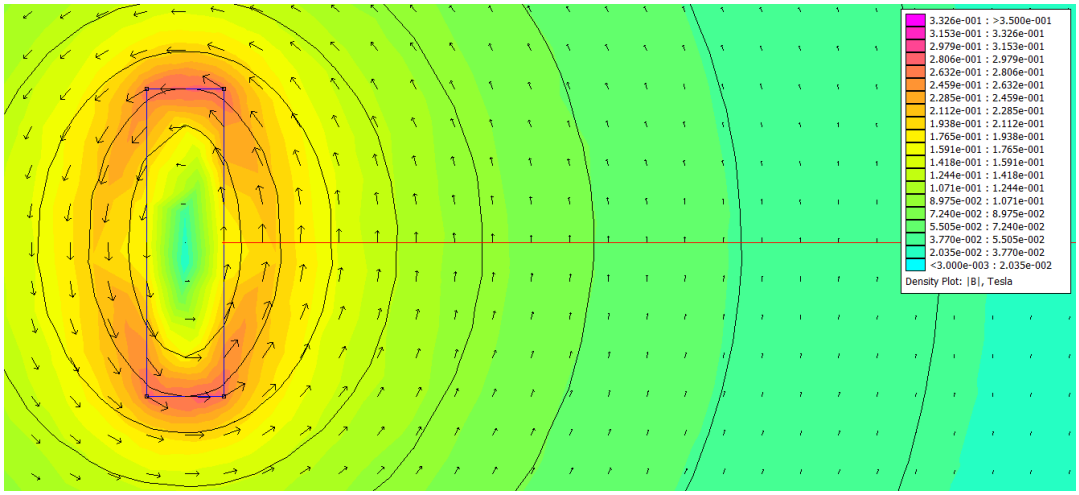

Figure 8: B Field Generated by a Rectangular Rail Carrying 20kA

And we plot the magnetic field in both instances to compare them as shown in Figure 9.

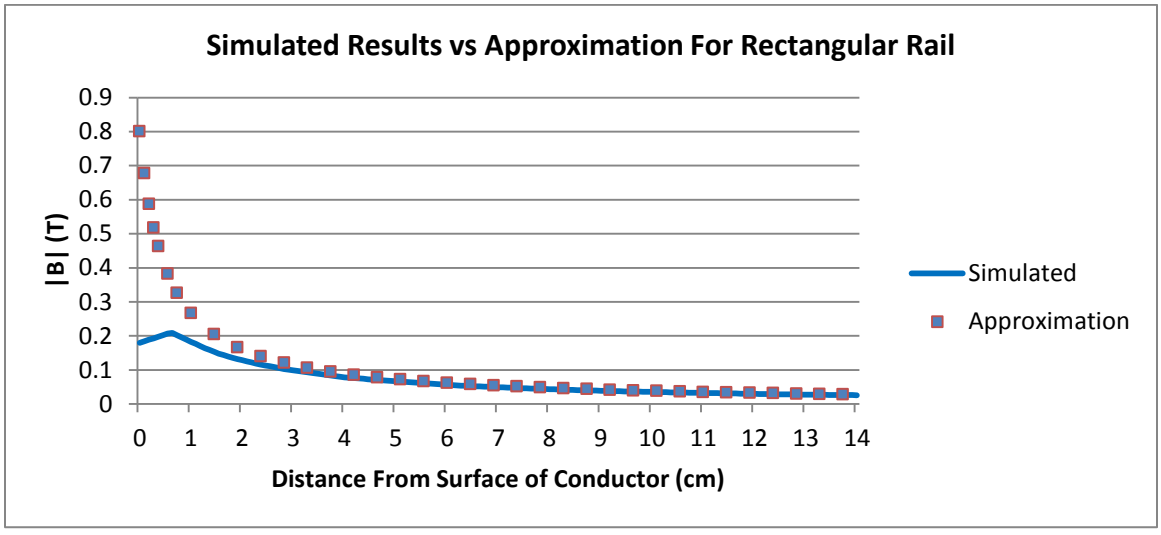

Figure 9: Comparison of Rectangle B field vs Approximate B field

In Figure 9 we can see a large difference between the simulated magnetic field near the rail and the predicted magnetic field via our approximation. The difference gets worse as the

length to width ratio of the rectangle strays farther and farther away from 1. Overall we can see that our approximation has the most trouble predicting fields near rails that don't have cylindrical geometry yielding in this case an average error of 20.9%.

This string of tests tells us that cylindrical rails have the best magnetic performance. Square rails in most cases are a close second but if rail spacing is close enough where only the magnetic field near the conductor falls on the projectile cylindrical rails can achieve significantly higher performance.

2.3 Describing Rail Force

We turn our attention to the scenario when two current carrying rails are brought within proximity of one another and carry the same amount of current as shown in Figure 10.

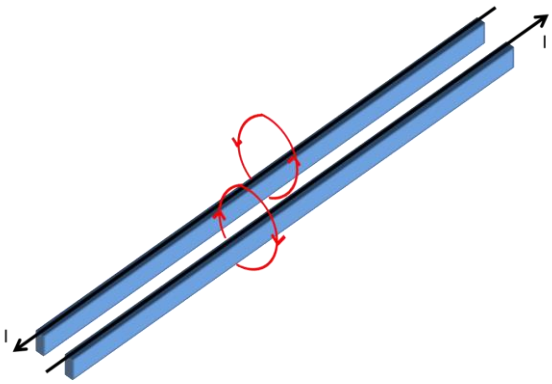

Figure 10: Parallel Rail Setup

If the currents are traveling in opposite directions as shown, using right hand rule, we determine the magnetic fields as depicted in red. If we apply the Lorentz force equation to this situation we'll find a force on each rail that is pulling it away from the other. Since these rails are parallel the magnetic field on one rail due to the other is nearly perpendicular to that rail. This means that the force on the rail can be approximated as:

$$\overrightarrow{F_r} \approx ILB \qquad \text{Equation 15}$$

Where I is the rail current, L is the length of the conducting rails, and B is the strength of the field at that point. However, as we found earlier the strength of the B field changes as you

move through space. If we break the wire up into an infinite number of pieces and multiply each by the local B field strength and conductor length, and then add them up we can get the total force. Since this is the very definition of an integral it is no surprise that an alternative way to write Lorentz force equation is:

$$F = I \int dl \times \vec{B} \qquad \text{Equation 16}$$

Since we have an expression for the magnetic field, we are going to derive an expression for the force each rail experiences in a setup identical to Figure 10. Figure 11 illustrates the framework that we're going to use.

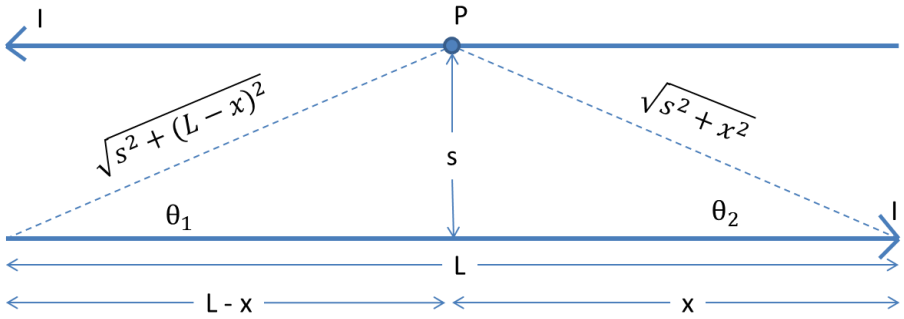

Figure 11: Parallel Rail Case

Applying Equation 14:

$$B(P) = \frac{\mu_0 I}{4\pi s}\left[\frac{L-x}{\sqrt{s^2+(L-x)^2}} + \frac{x}{\sqrt{s^2+x^2}}\right] \qquad \text{Equation 17}$$

Since the field is perpendicular to the rail the expression for $dl \times \vec{B}$ is:

$$dl \times \vec{B} = \frac{\mu_0 I}{4\pi s}\left[\frac{L-x}{\sqrt{s^2+(L-x)^2}} + \frac{x}{\sqrt{s^2+x^2}}\right] dx \qquad \text{Equation 18}$$

Thus Equation 19 transforms into:

$$F_r = \frac{\mu_0 I^2}{4\pi s}\left[\int_0^L \frac{L-x}{\sqrt{s^2+(L-x)^2}}\,dx + \int_0^L \frac{x}{\sqrt{s^2+x^2}}dx\right] \quad \text{Equation 19}$$

Let:

$$u = s^2 + (L-x)^2$$

$$du = -2(L-x)dx$$

$$v = s^2 + x^2$$

$$dv = 2xdx$$

Performing a “u” substitution and a “v” substitution on Equation 20 we get:

$$F_r = \frac{\mu_0 I^2}{4\pi s}\left[\int_{s^2+L^2}^{s^2} -\frac{1}{2}u^{-\frac{1}{2}}du + \int_{s^2}^{s^2+L^2}\frac{1}{2}v^{-\frac{1}{2}}dv\right] \quad \text{Equation 20}$$

$$F_r = \frac{\mu_0 I^2}{4\pi s}\left[-u^{\frac{1}{2}}\Big|_{s^2+L^2}^{s^2} + v^{\frac{1}{2}}\Big|_{s^2}^{s^2+L^2}\right] \quad \text{Equation 21}$$

$$F_r = \frac{\mu_0 I^2}{4\pi s}\left[-s + \sqrt{s^2+L^2} + \sqrt{s^2+L^2} - s\right] \quad \text{Equation 22}$$

$$\boldsymbol{F_r = \frac{\mu_0 I^2}{2\pi s}\left[\sqrt{s^2+L^2} - s\right]} \quad \text{Equation 23}$$

Equation 23 describes the force exerted on the rails as a function of the distance between them, the length, and the current passing through both of them. This rail force is important as a common problem in railgun design is the massive forces that tend to tear the gun itself apart. For example, a railgun with 1m long rails, separated by 2cm, and carrying 20kA will experience a force of about 3900N in total! We know exactly how parts of the rail design affect this parameter and what to be on the lookout for when selecting our design.

2.4 Finding the Projectile Force

We turn our attention to the projectile. Just like the rails we too are going to treat this as a zero volume conductor that is allowed to slide along the rails. Observing Equation 14 for the B field, we note that it weakens as you approach either end of a single rail. Now we assume that

our gun is sourcing current through a projectile that is sliding along the rails as depicted in Figure 12.

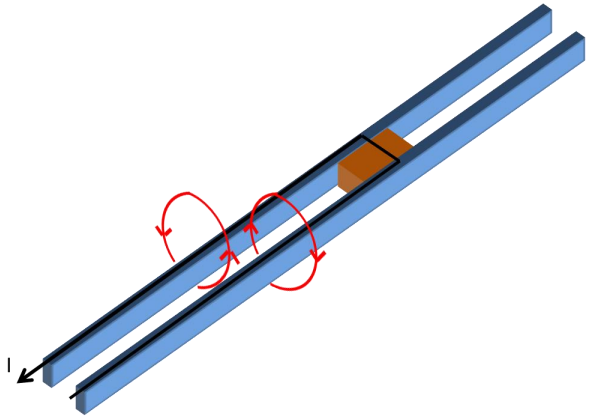

Figure 12: Standard Railgun Operation

In all equations thus far L has stood for the length of the rails that were conducting current. It is important to note that the physical rails are commonly longer than the L, however the length of rail that is not conducting current doesn't contribute to the rail magnetic field so we ignore it for magnetic calculations. If we wish to find the B field along the width of the projectile at any point we only need to know the current and how far down the rails the projectile is. Thus Figure 12 is simplified down into what is shown in Figure 13 with the two rails separated by a spacing of s carrying a current of I.

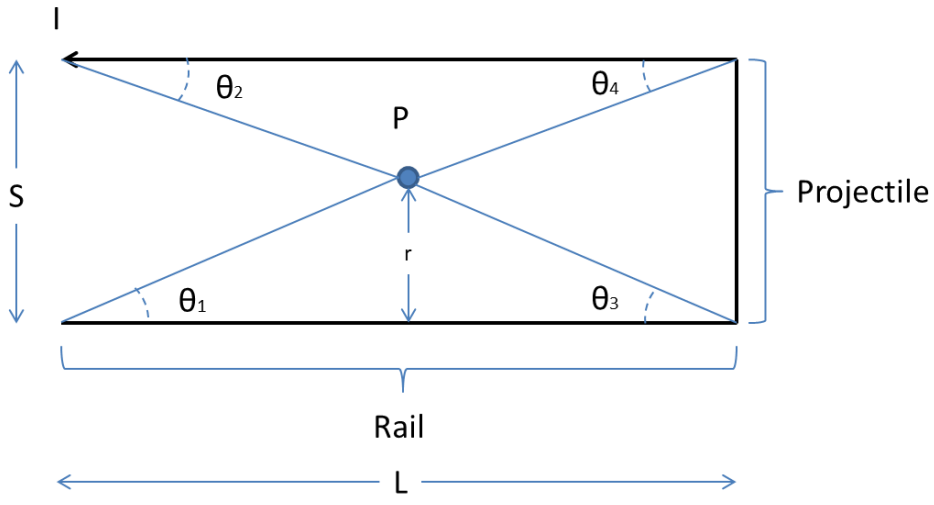

Figure 13: Simplified Geometry of a Railgun Used in Derivations

Looking at our expression for the B field due to one rail (Equation 14) we can see an expression for the B field due to two rails at a given point between the rails and in a plane they share is:

$$B(r) = \frac{\mu_0 I}{4\pi r}[\cos(\theta_1) + cos(\theta_3)] + \frac{\mu_0 I}{4\pi(s-r)}[\cos(\theta_2) + cos(\theta_4)] \ \ (0 < r < s) \qquad \text{Equation 24}$$

Where r is the shortest relative distance between the point on the projectile and the bottom rail, $\boldsymbol{\theta_1}$ and $\boldsymbol{\theta_3}$ correspond to angles formed by the bottom rail and lines drawn from the point to the ends of the bottom rail, and $\boldsymbol{\theta_2}$ and $\boldsymbol{\theta_4}$ correspond to angles formed between the top rail and lines draw from the point to the ends of the top rail. This is also due to the fact that the magnetic fields from each rail are parallel and easily add together. If we're measuring the B field along the projectile to the right one of the angles corresponding to each rail must be 90°. Thus Equation 25 for the B field along the projectile is:

$$B(r) = \frac{\mu_0 I}{4\pi r}\cos(\theta_1) + \frac{\mu_0 I}{4\pi(s-r)}\cos(\theta_2) \ \ (0 < r < s) \qquad \text{Equation 25}$$

To maximize the final velocity of the projectile we need to maximize the force on the projectile which means both I and the B field need to be maximized. To maximize the B field between the rails we must try to make $\theta_1 = \theta_2 = 0$ in Equation 25. This can very nearly be accomplished if we make L >> s. Thus the expression is:

$$\boldsymbol{B(r) \approx \frac{\mu_0 I}{4\pi r} + \frac{\mu_0 I}{4\pi(s-r)} \ \ (0 < r < s)} \qquad \text{Equation 26}$$

However, due to our assumption that the rails have zero width, the magnetic field approaches infinity as $r \to 0$ or $r \to s$ in Equation 26. This was employed to easily and accurately approximate the fields outside each rail. To find an accurate expression for the projectile force we must, and can easily account for the effects due to the non-zero width of the rails. The picture of this the new scenario is shown below in Figure 14.

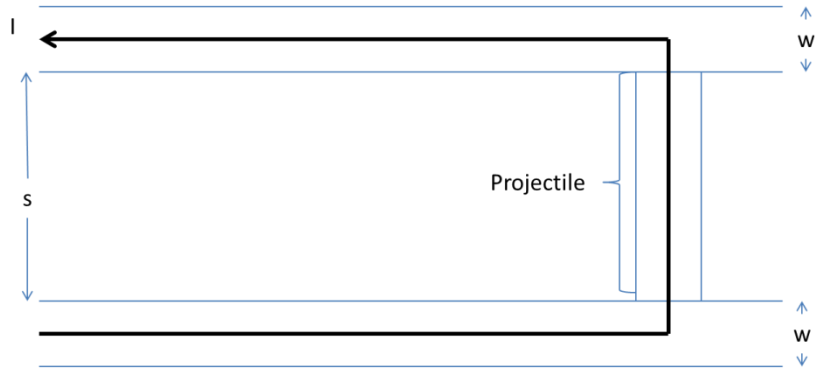

Figure 14: Non-zero Width Model

Using the Lorentz Force expression that incorporates current in Equation 15, the expression for projectile force is:

$$F = I\int_{\frac{w}{2}}^{s+\frac{w}{2}}\left(\frac{\mu_0 I}{4\pi r}+\frac{\mu_0 I}{4\pi(s+w-r)}\right)dr \qquad \text{Equation 27}$$

Where r is the distance measured from the inner side of the bottom rail to the inner side of the top rail and w is the width of the conductor. Continuing the evaluation of the integral in Equation 27:

$$F = \frac{\mu_0 I^2}{4\pi}\left[\int_{\frac{w}{2}}^{s+\frac{w}{2}}\frac{1}{r}dr+\int_{\frac{w}{2}}^{s+\frac{w}{2}}\frac{1}{(s+w-r)}dr\right] \qquad \text{Equation 28}$$

$$F = \frac{\mu_0 I^2}{4\pi}\left[\ln(r)\Big|_{\frac{w}{2}}^{s+\frac{w}{2}}-\ln(s+w-r)\Big|_{\frac{w}{2}}^{s+\frac{w}{2}}\right] \qquad \text{Equation 29}$$

$$F = \frac{\mu_0 I^2}{4\pi}\left[\ln\left(s+\frac{w}{2}\right)-\ln\left(\frac{w}{2}\right)-\ln\left(\frac{w}{2}\right)+\ln\left(s+\frac{w}{2}\right)\right] \qquad \text{Equation 30}$$

$$F = \frac{\mu_0 I^2}{2\pi}\ln\left(\frac{2s}{w}+1\right) \qquad \text{Equation 31}$$

Equation 31 is very important as it illustrates how the geometry of the gun directly influences the projectile force. It's not clear now but the geometry relation present in this

expression will become very important in future equations. Therefore for the rest of this paper K will be referred to as **projectile flux gain** denoted as:

$$\boldsymbol{K = \frac{\mu_0}{2\pi} \ln\left(\frac{2s}{w} + 1\right)} \qquad \text{Equation 32}$$

Thus Equation 32 can be rewritten as:

$$\boldsymbol{F = KI^2} \qquad \text{Equation 33}$$

2.5 Link Between Force and Inductance Gradient

The paper produced by the Naval Post Graduate School [11] instead defines F as:

$$F = \frac{1}{2} L' I^2 \qquad \text{Equation 34}$$

$$\text{Where } L' = \frac{\mu_0}{\pi} \ln\left[\left(\frac{2s+w}{w}\right)^2\right] \qquad \text{Equation 35}$$

This formulation is prevalent in literature discussing railguns; however it is only approximately true for the augmented rail design discussed in Chapter IV. The paper assumed the rail current travels through the entire length of the rail instead of the rail current terminating at the projectile's location. Therefore care must be taken when using the above expression. The correct formulation of Equation 35 doesn't square the argument of the natural log function above.

Equation 35 is often called inductance gradient because it describes the linear flux density between the rails per amp, far behind the projectile (assuming $\theta_1 = \theta_2 \approx 0$), and if L' is multiplied by the distance that the projectile travels we get the increase in flux per amp (Henry unit of inductance) due to the current loop becoming larger. In other words, it can be thought of as how fast the inductance increases as the projectile travels down the rails (with units of henries/meter). However this is misleading as it is only valid if the permeability of the space surrounding the projectile and the projectile itself is the same as the space around the rails.

Otherwise inductance gradient and projectile force are not necessarily tied together by Equations 32-35 as will be shown later.

2.6 Circuit Modeling

We now model the system as an electric circuit. The motional electromotive force, which is the voltage induced in a rod that is moving through a perpendicular magnetic field, is given by:

$$E = lv \times B \qquad \text{Equation 36}$$

Where E is the voltage induced, v is the velocity of the rod, and B is the B field that immerses the rod. Using the same situation in Figure 8 the expression for the emf of the projectile is:

$$E = v \int B \, dL \qquad \text{Equation 37}$$

Since the B field changes along the length of the projectile we proceed to divide up the projectile along the width, multiply each piece by the local B field, and add up all of their contributions. For this purpose we use an integral shown in Equation 37. Since we are integrating the B field over the same length as the projectile force integral we can use part of the result to get the expression:

$$E = KIv \qquad \text{Equation 38}$$

So we can use a resistor to model total system resistance, a voltage source forcing current into the rails, and a voltage source opposing the flow of current as shown in Figure 15.

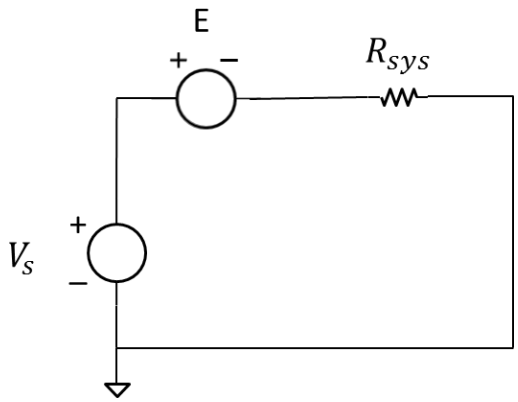

Figure 15: Derived Model Circuit With Back-EMF

The projectile's emf can be thought of as a current controlled voltage source whose gain is determined by Kv. If we divide both sides of Equation 38 by the rail current it is obvious that this voltage source behaves as a resistor. Thus the new circuit can be redrawn as shown in Figure 16.

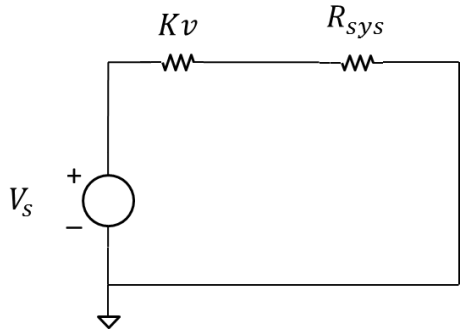

Figure 16: Equivalent Model Circuit

This model is easier to work with since it represents a simple voltage source in series with a constant resistor and a variable resistor that scales with the K value of the system and the velocity of the projectile. The variable resistor and the K value of the system are the most complicated aspects of the system and having them summed up by a simple analytical expression is very valuable during the design process. This resistor is also a major source of the system's non-linearity since its value increases as current passes through it over time. We now can see an expression for the instantaneous efficiency of the system. That is, an expression for the efficiency given the state of the machine at a specific point:

$$\eta = \frac{Kv}{Kv+R_{sys}}$$ Equation 39

Equation 39 shows that as the velocity of the projectile increases the efficiency of the machine increases assuming R_{sys} stays constant. This suggests that a good design requires that the projectile has very high initial velocity before it conducts across the rails. This also shows that a high K value of the design leads to even higher efficiency even at lower velocities – another important design parameter. It's important to mention that K values for most practical designs are typically on the order of 10^{-6}. Since K increases on a logarithmic scale as the distance between the rails widens it is difficult to increase through gun geometry alone. One can try to alter μ_0 (by using different materials) to potentially increase K by hundreds of times, but magnetic saturation limits the actual gain in K under the high currents that railguns typically operate on. However R_{sys} can vary dramatically and can be lower than 1mΩ, and as high 60mΩ just through capacitor equivalent series resistance (ESR) and inductor DC resistance (DCR) alone. Therefore most gains in efficiency are realized by lowering R_{sys}. This is the reason that some designs choose the Vsource that powers their circuit to be just a capacitor bank due to the (often) very low ESR and very high power output.

2.7 Final Projectile Velocity

Now we're going to assume a fully charged capacitor is powering the circuit in place of Vsource as shown in Figure 17 and analyze the resulting circuit the moment the capacitor is allowed to discharge through the resistor.

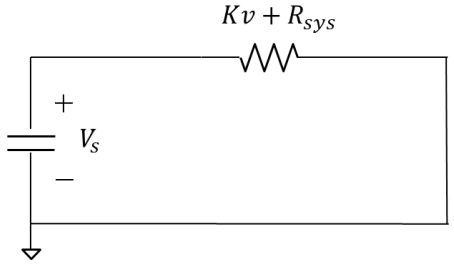

Figure 17: Simplified Electric Model for Capacitor Powered Railgun Circuit

We want to find the velocity of the projectile once all of the energy in capacitor has been released. In an RC circuit we can assume all of the energy stored in the capacitor is dissipated by the resistive components in the circuit thus:

$$E_c = \int_0^\infty \left(R_{sys} + Kv\right) I^2 dt \qquad \text{Equation 40}$$

Where E_c in Equation 40 is the stored energy in the capacitor. Substituting our expression relating force and current the above expression becomes:

$$E_c = \int_0^\infty (R_{sys} + Kv) \frac{F}{K} dt \qquad \text{Equation 41}$$

$$E_c = \int_0^\infty (R_{sys} + Kv) \frac{ma}{K} dt \qquad \text{Equation 42}$$

$$E_c = \frac{m}{K} \int_0^\infty (R_{sys} + Kv) \frac{dv}{dt} dt \qquad \text{Equation 43}$$

$$E_c = \frac{m}{K} \int_{v_0}^{v_f} (R_{sys} + Kv) dv \qquad \text{Equation 44}$$

$$E_c = \frac{m}{K} \left(R_{sys}(v_f - v_0) + \frac{1}{2} K (v_f^2 - v_0^2) \right) \qquad \text{Equation 45}$$

$$-\frac{1}{2} m v_f^2 - \frac{m R_{sys}}{K} v_f + \frac{m}{K} R_{sys} v_0 + \frac{1}{2} m v_0^2 + E_c = 0 \qquad \text{Equation 46}$$

$$v_f = \frac{\frac{m R_{sys}}{K} \pm \sqrt{\left(-\frac{m R_{sys}}{K}\right)^2 - 4\left(-\frac{1}{2} m\right)\left(\frac{m}{K} R_{sys} v_0 + \frac{1}{2} m v_0^2 + E_c\right)}}{-m} \qquad \text{Equation 47}$$

$$\boldsymbol{v_f = -\frac{R_{sys}}{K} + \sqrt{\left(\frac{R_{sys}}{K}\right)^2 + 2\left(\frac{R_{sys} v_0}{K} + \frac{1}{2} v_0^2 + \frac{1}{m} E_c\right)}} \qquad \text{Equation 48}$$

Since this velocity corresponds to the point in time where all of the energy stored in the capacitor has been spent we may regard Equation 48 as an expression for the final velocity of the projectile. Equation 48 is very important as it shows that gun geometry directly impacts the final velocity of the projectile given the capacitor's size and initial voltage.

To get a better understanding let's set R_{sys} = 0 in Equation 48. The above expression becomes:

$$v_f = \sqrt{\left(v_0^2 + \frac{2}{m}E_c\right)} \quad \text{Equation 49}$$

$$KE_{final} = \frac{1}{2}mv_f^2 = \frac{1}{2}mv_0^2 + E_c \quad \text{Equation 50}$$

Using the definition of kinetic energy ($KE = \frac{1}{2}mv^2$) we see that the projectile's final kinetic energy is:

$$KE_{final} = KE_{initial} + E_c \quad \text{Equation 51}$$

If the system's resistance is zero then we'll always achieve 100% efficiency. This is impossible to achieve in practice, but at least theoretically as R_{sys} becomes smaller we get closer to that reality. We want all the power to be dissipated over the Kv resistor and minimal amount if possible to be dissipated over R_{sys} in a real system. Another aspect to note is how K and R_{sys} are tied together. Notice in Equation 48 that large K has the same effect as small R_{sys}. Doubling K yields same increase in efficiency as halving R_{sys}. This fact is important because again Equation 32 tells us that K is hard to increase through the gun's geometry, but Rsys can vary easily by orders of magnitude. The ratio of R_{sys} to K can tell us the efficiency of a design without knowing anything physical about the gun itself and the final projectile velocity assuming all of the energy is dissipated.

An alternative way to write Equation 48 is:

$$v_f = -\frac{R_{sys}}{K} + \sqrt{\left(\frac{R_{sys}}{K}\right)^2 + 2\left(\frac{R_{sys}v_0}{K} + \frac{1}{m}\left(\frac{1}{2}mv_0^2 + E_c\right)\right)} \quad \text{Equation 52}$$

$$\boldsymbol{v_f = -\frac{R_{sys}}{K} + \sqrt{\left(\frac{R_{sys}}{K}\right)^2 + 2\left(\frac{R_{sys}v_0}{K} + \frac{1}{m}(KE_{inital} + E_c)\right)}} \quad \text{Equation 53}$$

This may make it easier to understand what's happening and just how dominant that ratio is when finding the final velocity.

Finding an analytical expression for the voltages and currents in such circuit has proven to be challenging because of the non-linearity introduced into the system by the resistor representing the back EMF. We have turned to MATLAB simulation for solving the necessary non-linear integro-differential equations to determine how far the projectile travels once all of the energy in the capacitor has been discharged. Using Simulink we can find the rail length required for the capacitors to completely discharge before the projectile leaves the rails.

2.8 Rail Inductance

One final aspect we should analyze is the effects of inductance in the system. As mentioned back in section 2.4 the max inductance of the railgun can be found by multiplying L' by the rail length. To see the impact of finite rail inductance we simulated the best case and worst case scenario and compared them. Since this is an RLC circuit the rise time will be worse and we may get some transient oscillations [8]. These currents only matters if the capacitors are polarized because the reverse currents may destroy them by reverse biasing the capacitor voltage and the currents may be large enough to destroy a flywheel diode (diode in parallel with capacitor that prevents the capacitor voltage from dropping too low) meant to protect the capacitors. To prevent these currents we ensure that [8]:

$$\zeta = \frac{R}{2}\sqrt{\frac{C}{L}} \geq 1 \qquad \text{Equation 54}$$

A particularly bad scenario uses the lowest possible ESR of a capacitor that could be found (.00023Ω) as the R_{sys} and a capacitor with an energy capacity of 1kJ. We want Equation 54 to be valid. Figure 18 shows a circuit with ζ = .0727 with the capacitor voltage shown in Figure 19.

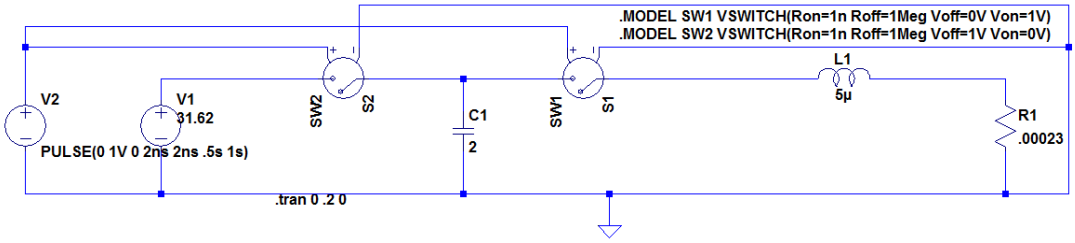

Figure 18: Circuit Schematic

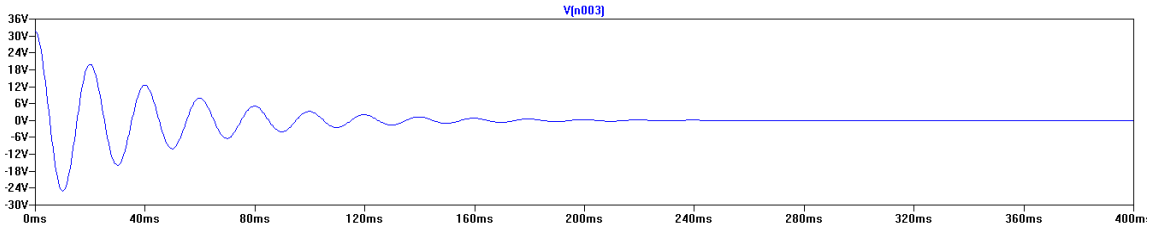

Figure 19: Discharging Capacitor Voltage

The above was simulated using LT spice IV. The V1 source is responsible for charging the capacitor in Figure 18. SW1 turns on if V2 is one volt and off if V2 is zero, and SW2 is vice-versa. The .MODEL statements configure the switches turn on/off voltages as wells as their off and on resistances which are set to 1MΩ and 1nΩ respectively. V2 is a 50% duty cycle rectangular pulse with rise and fall times of 2ns and a period of 1s.

As we can see there is a very large oscillation in capacitor voltage accompanying the large reverse current in the circuit. To see this, take the derivative of the voltage waveform above and multiply it by the capacitance of the capacitor. However, if we change this circuit such that the energy stored in the capacitor remains the same and $\zeta = 1$ (shown in Figure 20) we see that the output has a longer discharge time and no oscillating as shown in Figure 21.

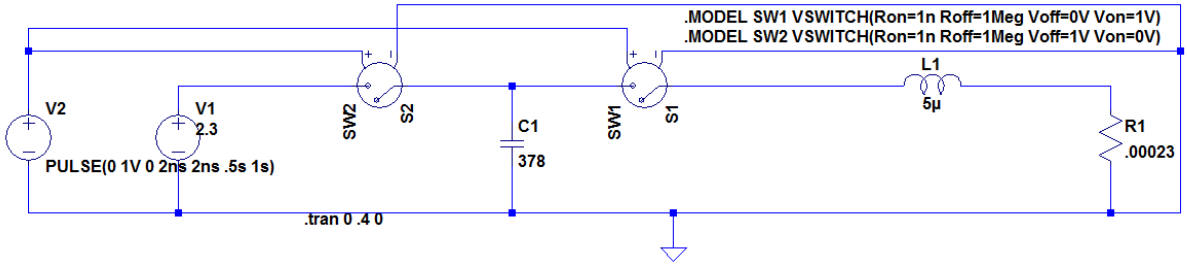

Figure 20: Circuit Schematic With $\zeta = 1$

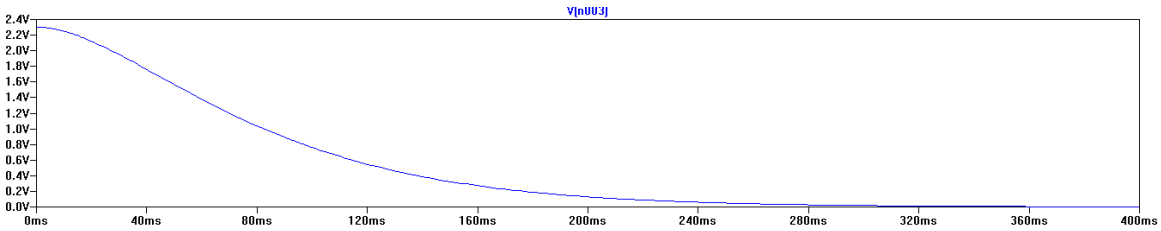

Figure 21: Effects of Altered ζ

So this is one way to reduce potential oscillations if that is desired at the likely cost of increasing the discharge time. We wish to see the effects of the inductance on final projectile velocity once all of the energy has been dissipated over the resistive elements if any. Since all of the system's energy is dissipated over the resistive part of the circuit even with an inductor, our previous analysis still holds true. Note that the expression for the final velocity of the projectile is still Equation 48. The change in projectile velocity only depends on K, m (mass of projectile), E_c, V_0, and R_{sys}. Adding an inductor won't change the final velocity of the system because none of these the values in Equation 48 are altered.

3 System Simulation

A set of equations that describe the system's behavior have been developed and it is time to solve them. As mentioned in section 2.6, the railgun is a non-linear system so to get accurate answers based on the equations developed thus far we must use differential equation solvers that can approximate the actual solution as close as possible. In total we're going to need 3 major subsystems, one to calculate the K value based on physical and magnetic properties of the gun, one to calculate the current going through the rails based on the state of the machine, and another to carry out the rail force calculation all of which are non-linear. Once those figures are determined the projectile force and many other parameters can easily be computed by integrating them and multiplying them by constants. Shown below in Figure 22 are all of the necessary simulink blocks that will be needed to accomplish that and display the results.

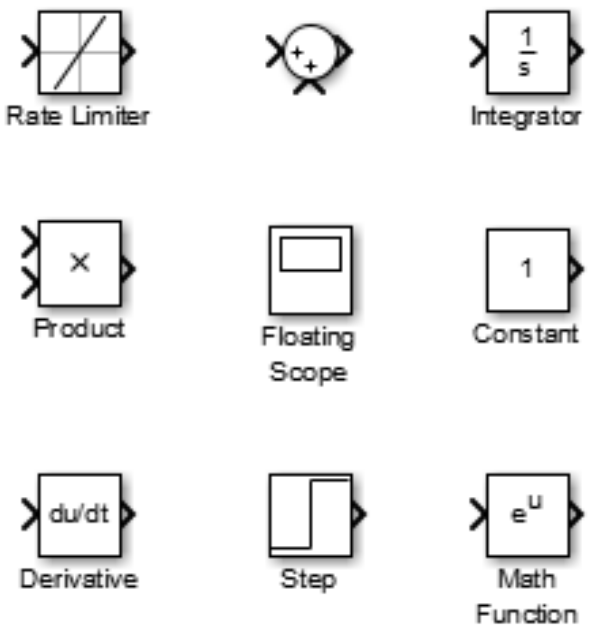

Figure 22: Computation Blocks Used

The rate limiter block is used in conjunction with the step function. The reason for this is to ensure that the derivative of the step function is well defined and doesn't cause errors when passing through the derivative block which takes the derivative of the incoming signal and outputs the result. To ensure there are no initialization errors with the blocks at t=0s we delay the step

function by 1μs. The constant block outputs a constant signal at the level specified by the defined value. The product block multiplies incoming signals but allows each port to be configured as a multiplier or a divider. So the product block really carries out multiplication and dividing operations. The floating scope plots the signal that feeds into it over time as the simulation runs. The integrator integrates the incoming signal and outputs the result. The math function block runs its input through a choice of functions and then outputs the result. The remaining block is a summing junction that can add or subtract signal by summing signals that are multiplied by 1 (+) or -1 (-) as indicated on the block.

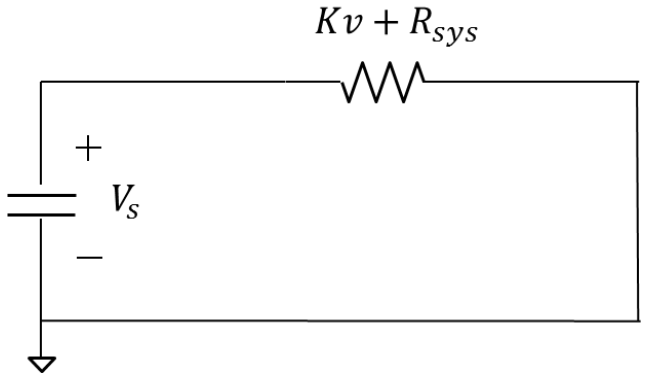

Figure 23: Simplified Equivalent Circuit for Railgun

The equivalent circuit of a railgun can be modeled as a non-linear RC circuit as shown in Figure 23. The current conducted by this RC circuit:

$$I = -\frac{dv_s}{dt}C \qquad \text{Equation 55}$$

The negative sign is due to the current leaving the positive terminal of the capacitor. Solving for the voltage of the capacitor we find:

$$v_s = -\frac{1}{C}\int Idt + v_c \qquad \text{Equation 56}$$

Where v_c is the initial voltage of the capacitor. However:

$$I(t) = \frac{v_s}{R_{sys}+Kv} = -\frac{1}{(R_{sys}+Kv)C}\int Idt + \frac{v_c}{(R_{sys}+Kv)} \qquad \text{Equation 57}$$

We see that there are going to be multiple feedback paths due to the velocity and the current in the capacitor. These equations form the basis of the subsystem responsible for finding the current. We focus first on the capacitor, Figure 24 below shows how one can implement a system that the above equation describes in MATLAB's Simulink:

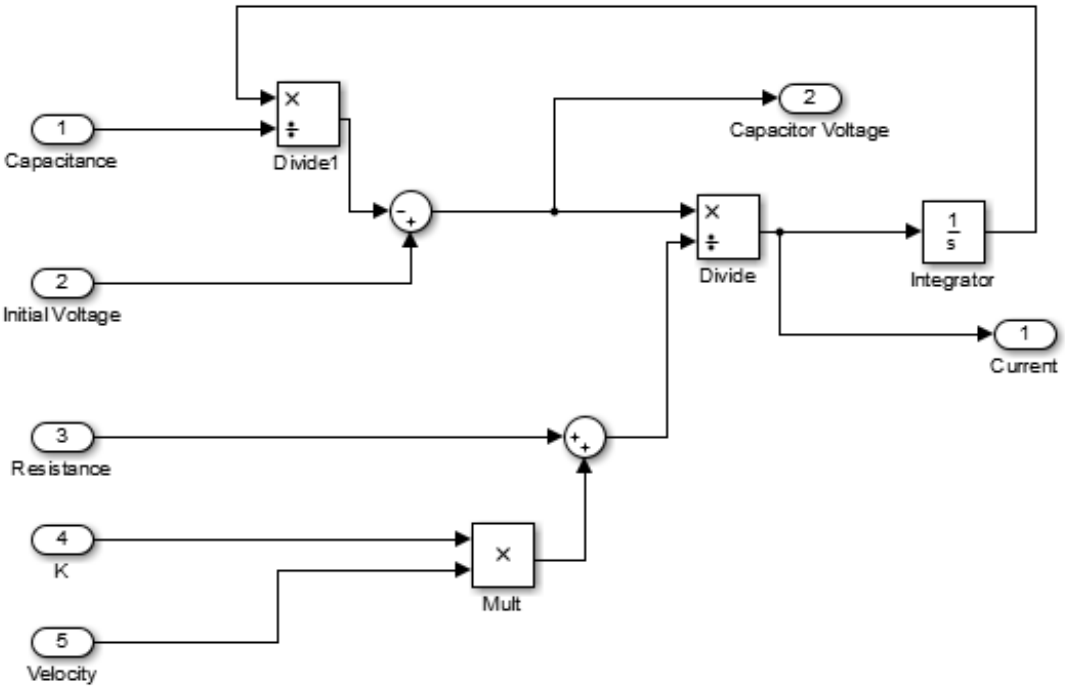

Figure 24: MATLAB Simulink Modeling Capacitor Current

We can see the feedback path starting where the current probe is. The signal is integrated, divided by C, subtracted from the initial voltage and then divided by circuit resistance before repeating again. The velocity signal will be changing and is the only other dynamic component in this system.

Before in section 2.8 we ignored the effects of inductance introduced into the system due to the current loop formed by the rails, power source, and projectile. If possible we would like to include the effects of nonzero inductance within the simulation. To see how to do this we first state the governing equation of an inductor as:

$$v_L = \frac{di}{dt}L$$ Equation 58

Adding an inductor into the existing system would change the voltage over the resistor by:

$$v_R = v_S - \frac{di}{dt}L$$ Equation 59

Therefore we can take the result for the current, differentiate and multiply it by L, and then subtract the result from the part of the system that finds the capacitor voltage. The modified subsystem is shown below in Figure 25.

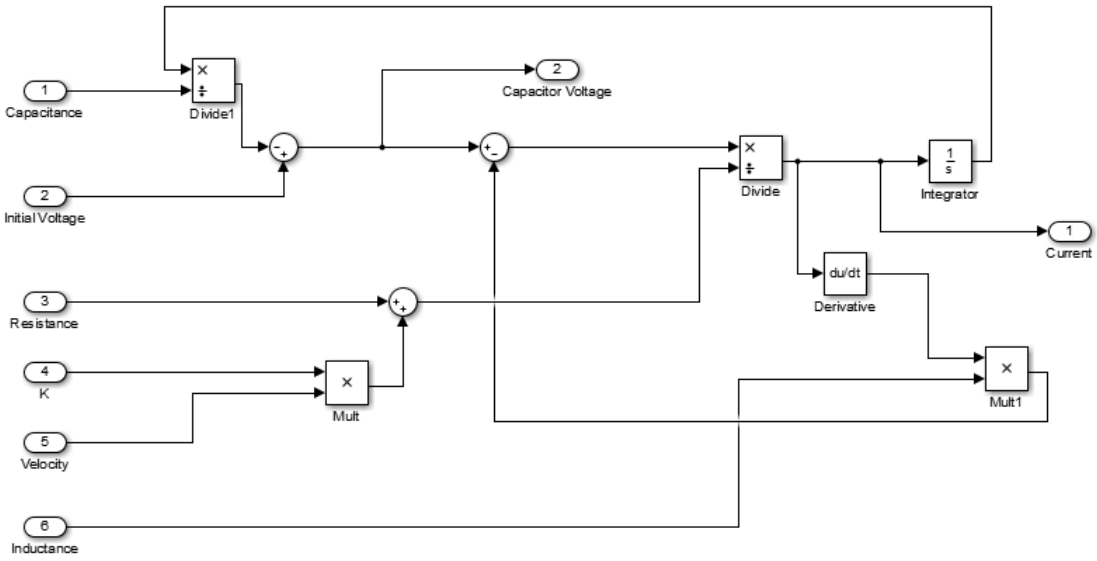

Figure 25: MATLAB Simulink RLC Railgun Circuit Model

The rest of the system follows directly from the Equations 23, 32, 33. Below shows the part of the simulator that sums all the forces (gravity force is included for the case of the projectile propelled upward) in Figure 26.

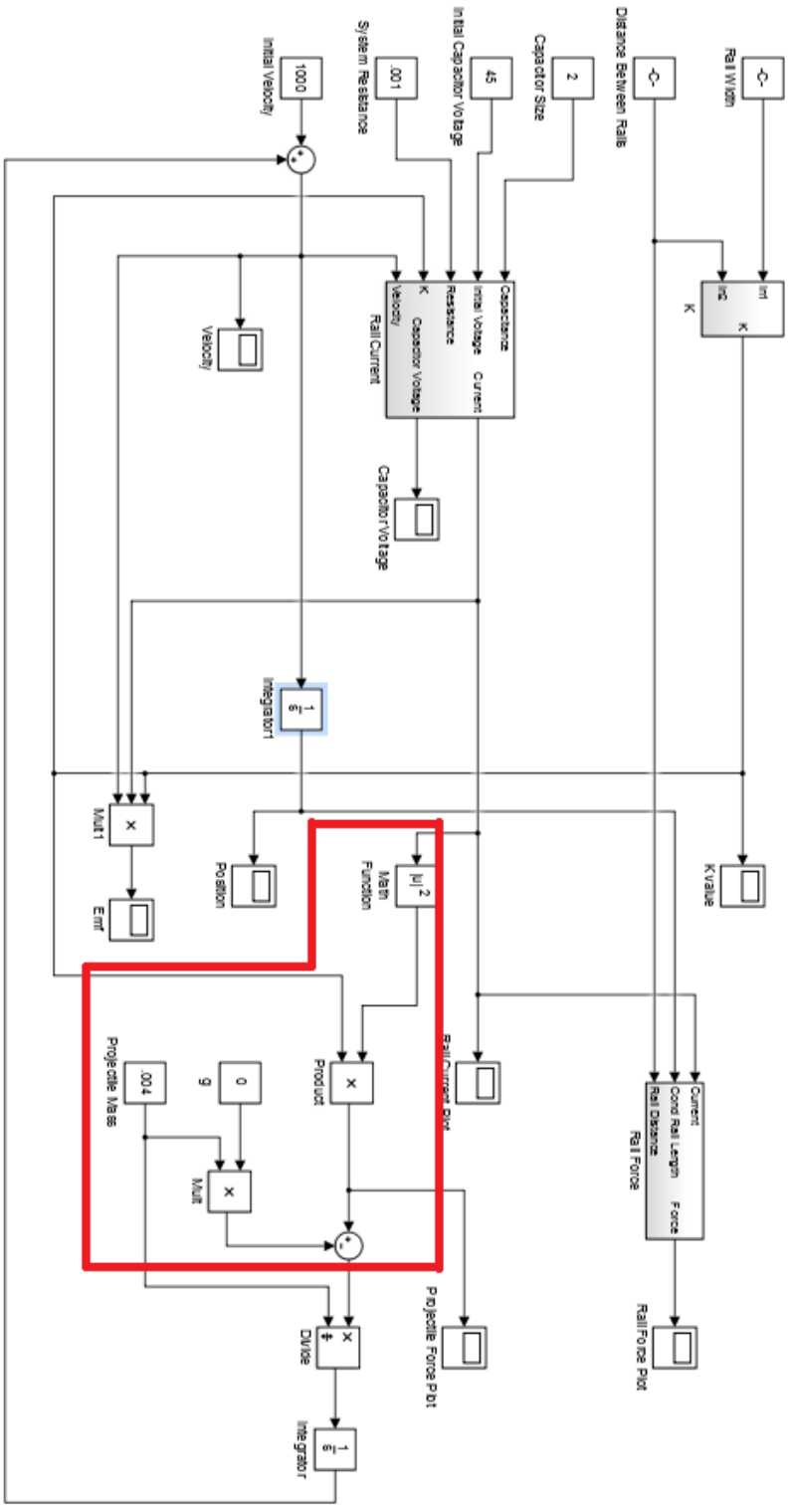

Figure 26: Summation of Forces Section of Simulator

The K subsystem performs the calculation (Equation 33) necessary to find the K value which is used in the EMF and projectile force equations. The Rail Forces subsystem calculates the rail force (using Equation 24) over time given rail spacing, current, and conducting length. The Mult1 block calculates the back emf of the system.

The complete system for the simulator to solve is shown below in Figure 27. The core gain factor will be explained in detail later, but for now know that it attempts to capture the effects of using materials with a relative permeability $\mu_r > 1$ for or near the projectile.

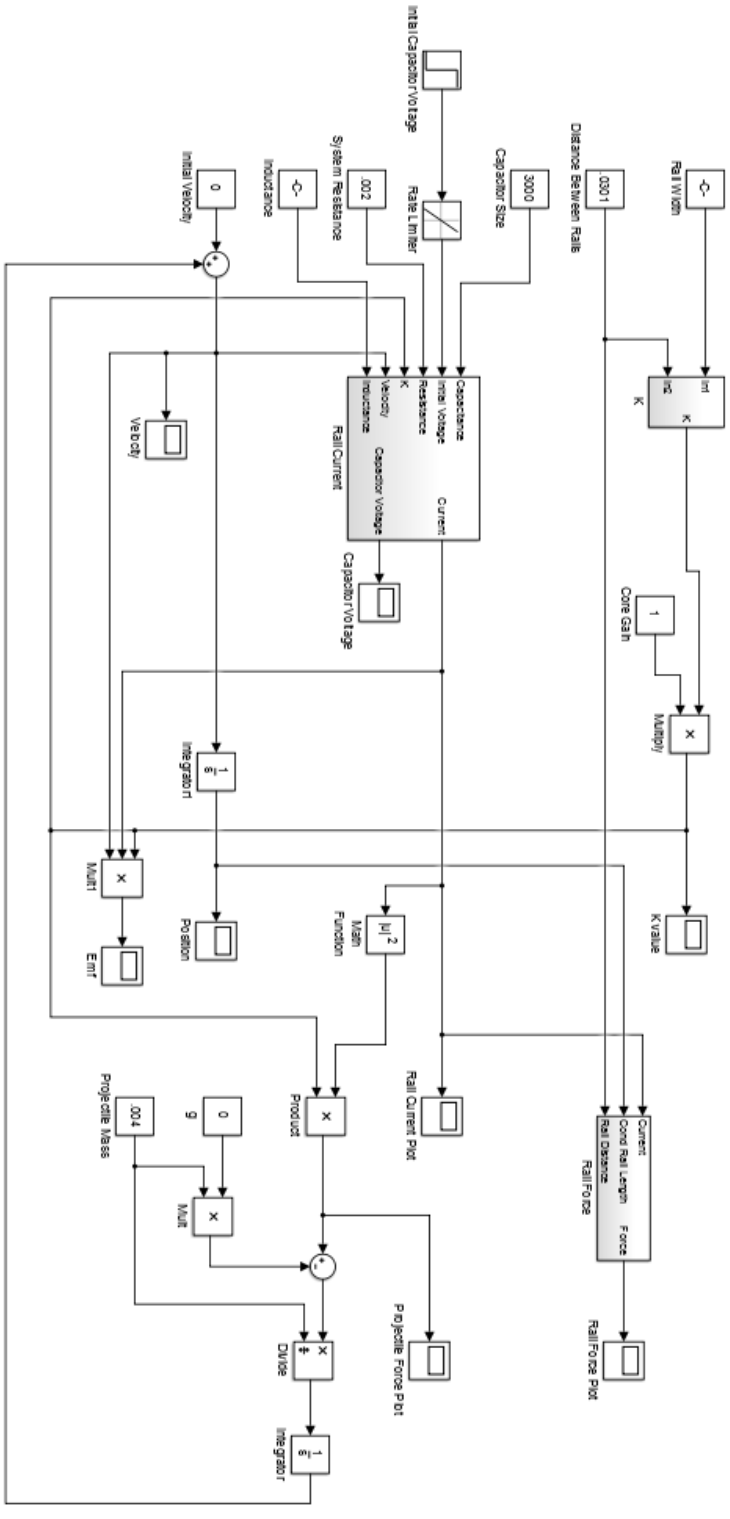

Figure 27: Complete System Overview

For clarity the circuit model which includes the inductance introduced by the current loop formed by the projectile, rails, and power source is shown below in Figure 28.

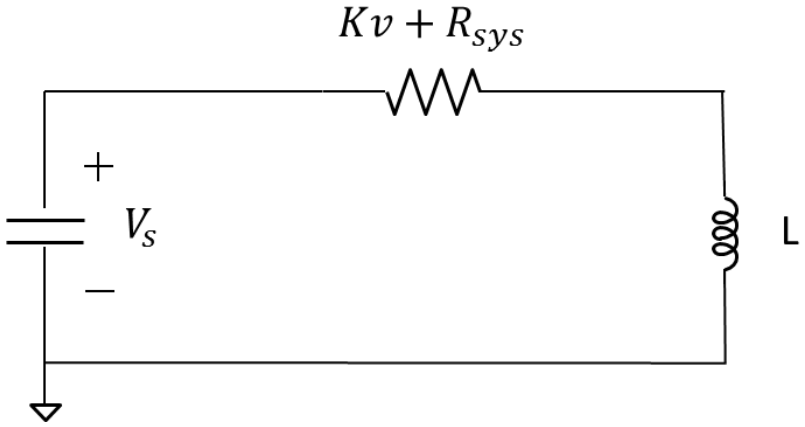

Figure 28: Complete Circuit Model

3.1 Verification of Conclusions Regarding Efficiency and Inductance

Using the developed model we can simulate and plot the projectile's position, velocity, rail forces and back EMF over the duration of the firing period for the launcher. To ensure the simulator is working as theorized let's substitute in some values and see the results of the projectile's velocity. Remember we said that as the projectile travels faster the machine becomes more efficient and takes longer for the capacitor to discharge completely. Below Table 1 and Figure 29 shows the values and the projectile velocity output. Figure 30 shows the results for the values shown in Table 2. To keep the analysis simple we'll ignore gravity by setting g in the simulator to 0.

Table 1: Base Case Simulation Values

Rail Width	.00635m
Distance Between Rails	.0254m
Capacitor Size	2F
Initial Voltage	10V
System Resistance	.001Ω
Inductance	0H
Initial Velocity	0m/s
g	$0m/s^2$
Projectile Mass	4g
Core Gain	1
Simulation Runtime	.6s

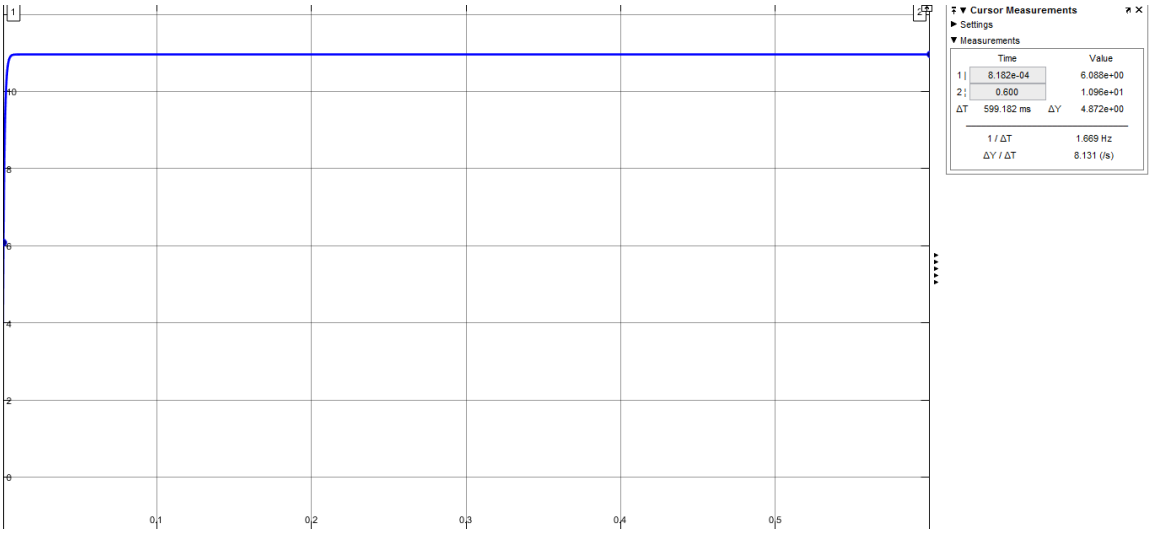

Figure 29: Base Case Projected Velocity With Zero Initial Velocity

It takes approximately 5.8ms for the projectile to reach its maximum speed of 11 m/s giving the projectile a kinetic energy of .242J and an efficiency of .242%. However if we provide the projectile a large initial velocity the effects of the back emf become more noticeable with the projectile taking longer to reach it peak velocity. Below is the velocity plot of the same railgun with a 10000m/s initial velocity (little over 30 times the speed of sound).

Table 2: 10,000m/s Initial Velocity Simulation Values

Rail Width	.00635m
Distance Between Rails	.0254m
Capacitor Size	2F
Initial Voltage	10V
System Resistance	.001Ω
Inductance	0H
Initial Velocity	10,000m/s
g	$0m/s^2$
Projectile Mass	4g
Core Gain	1
Simulation Runtime	.6s

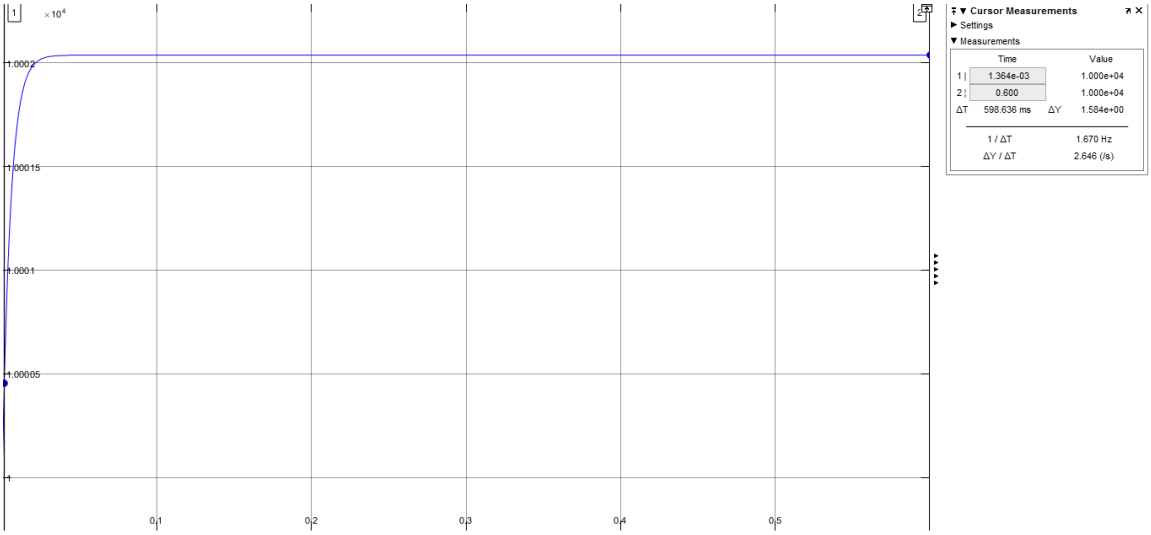

Figure 30: Velocity Plot With Initial Velocity of 10,000m/s

Now the back emf effect is very clear. It takes around 30ms for the capacitor to completely empty its energy this time with the final velocity of the projectile approximately 10002.03m/s. The amount of energy that was converted into kinetic is 81.2J. Since the potential energy of the potential energy stored in the charged capacitor was still at 100J this yields an efficiency of 81.2%. The initial velocity had to be high in this case to see the effects because the K value of this system is around 4.39×10^{-7}. The resistance of this system is 1mΩ and the Kv resistor in our model circuit shown below is nearly 5 times higher than the static system resistance. The circuit looks like an RC circuit with a time constant that is 6 times larger which is

reflected in the projectile velocity over time. As stated in Equation 39, efficiency increases with projectile velocity so the simulation is matching our understanding so far.

One more test will be run and only differs from the base case by setting L=100μH. The results are shown below in Figure 31.

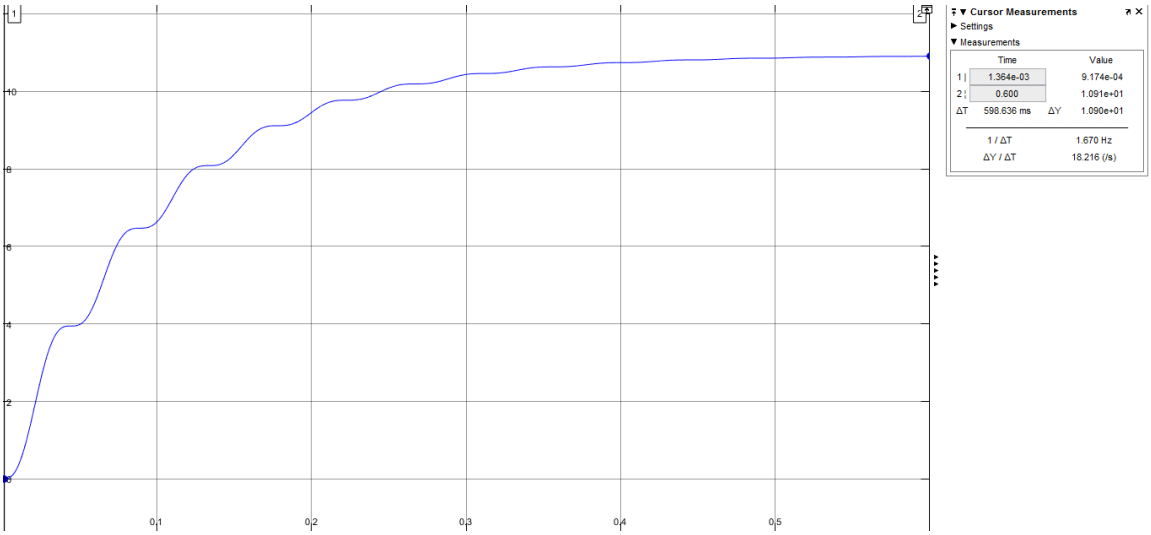

Figure 31: L=100μH Result

Also worth noting is how the final velocity of the projectile didn't change even with the additional inductance added to the circuit as claimed back in section 2.8.

4 Possible Designs of Railguns

The idea of a railgun has been around for nearly 100 years [3], however for most of that time we just didn't possess the necessary electronics or materials to make it feasible. Shown below in Figure 32 is the typical design of railgun [11].

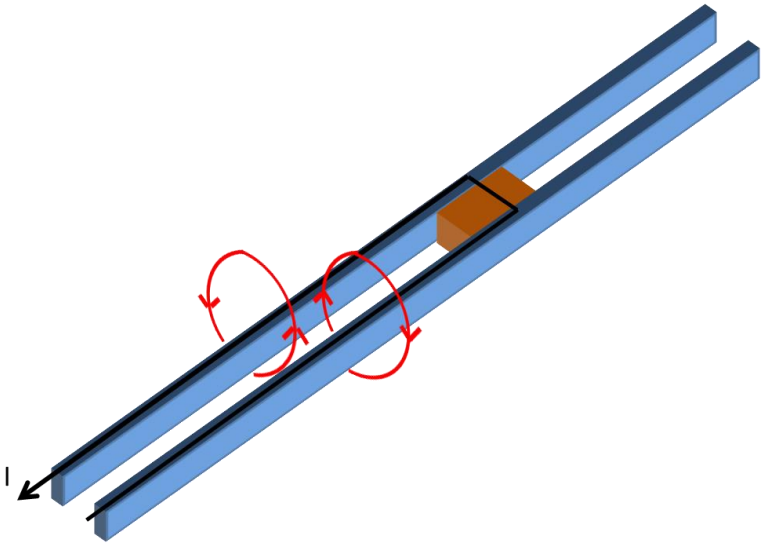

Figure 32: Typical Railgun Design

Just because it's easy to find doesn't make it the best design for every application. As discussed back in section 2.2, round rails provide a stronger average magnetic field over the projectile to maximize the force acting on it while the common picture above usually depicts square rails. Typically bracing for the rails is also missing which turns out to be a serious matter for some designs. There are many designs that won't work because the massive rail forces will split the device down the axial direction [11]. Another problem is that the rail forces will cause the rails to deflect slightly outward which can introduce large enough air gap to break the electrical contact between the rails and the projectile, increasing the impedance of the rails. This tends to be another factor that can destroy the performance of designs once implemented.

4.1 Augmented Rail Design

Another design occasionally mentioned is the augmented rail design [10]. Instead of using just two rails, we use a multiple of two rails and stack them together side by side on each side of the projectile. Figure 34 illustrates what this configuration might look like.

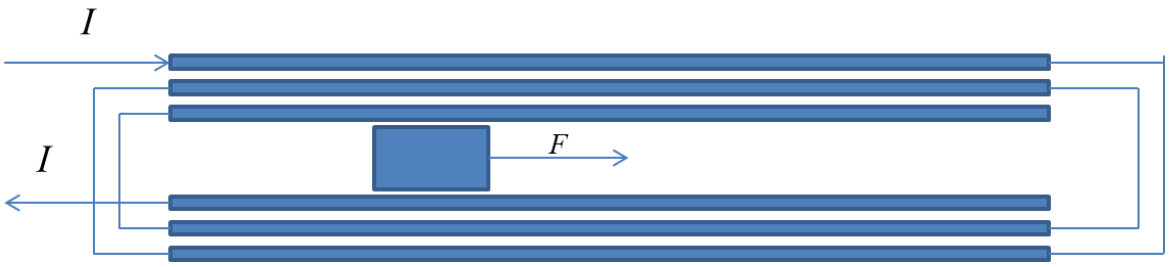

Figure 33: Augmented Rail System

Figure 34 has the advantage of generating more force for the given current compared to the typical design. The original rail system (Figure 32) could be thought of as a single turn inductor and Figure 34 results if we increase the number of turns past one. Approximately, the total flux generated by the rails is that of a single set of rails multiplied by the number of turns. This means the K value and rail force for the system is roughly multiplied by the same factor.

However this is a case of diminishing returns as stacking rails also leads to the projectile being farther and farther away from the outer rails. This means that while the outer rails contribute to the total flux through the projectile, they contribute less than the inner rails. Therefore the rails need to be as thin as possible to minimize this effect. There is also the issue of properly insulating the rails to ensure that the current travels around the rail system as intended. If the system voltage is high enough insulating the rails can become a looming issue. This insulation must also be kept as thin as possible as it can lead to the outer rails being too far away from the projectile [10].

Making the rails very thin and running current through longer lengths of rail also drastically increases the system resistance which is a source of losses in efficiency according to Equation 39 and power output, the two metrics that we're trying to maximize.

4.2 Magnetic Shell Design

The final design considered works best with a non-magnetizable projectile as very little gain in railgun performance is realized with a magnetic projectile. The projectile sits in the rails as shown in Figure 35 and is surrounded by an iron (or other magnetic material) shell.

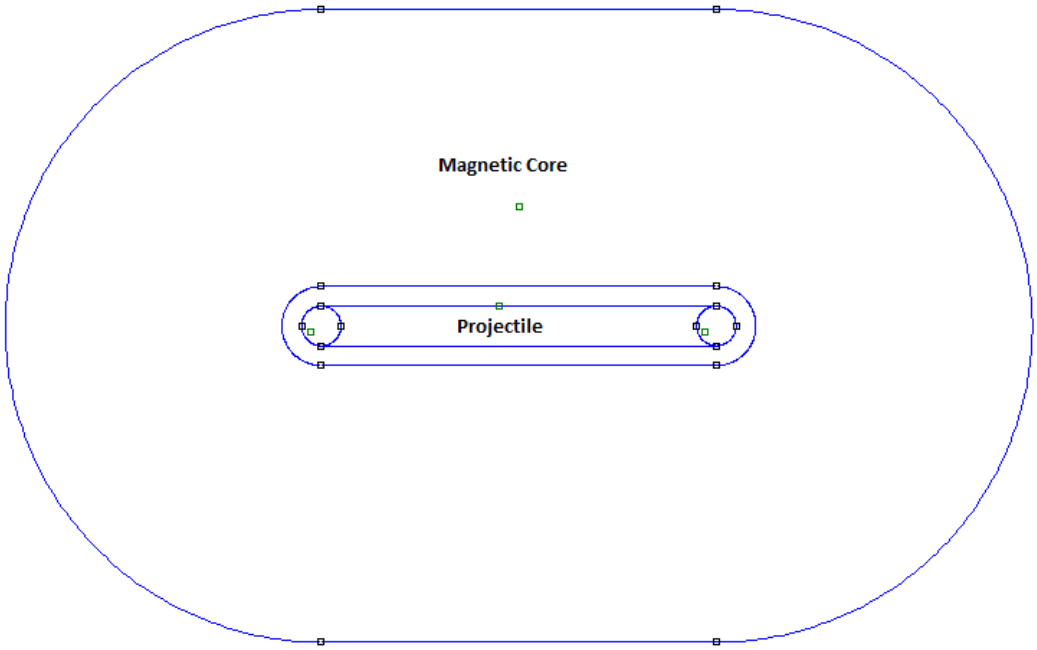

Figure 34: Magnetic Shell Railgun

Most of the H field that the rails generate will fall over the small air gap where the projectile sits. This leads to potentially hundreds of times more flux being generated where the projectile sits than without the iron shell when comparing Figure 36 and Figure 37. These simulate .25” in diameter copper rails carrying 10kA of current and ideally there is some insulation to electrically isolate the rails from the shell.

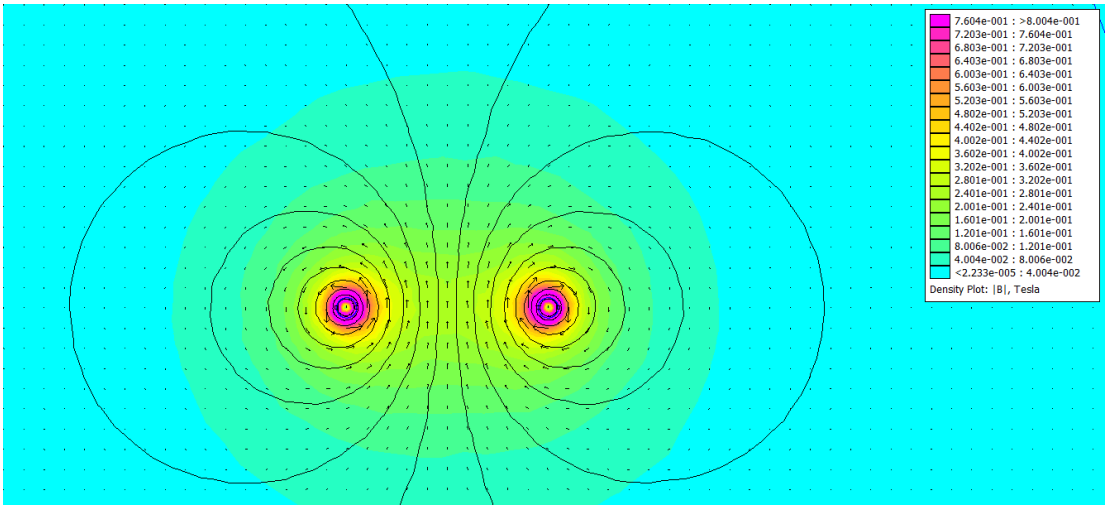

Figure 35: Typical Rail Setup (Average Flux Density Between Rails = .257 T)

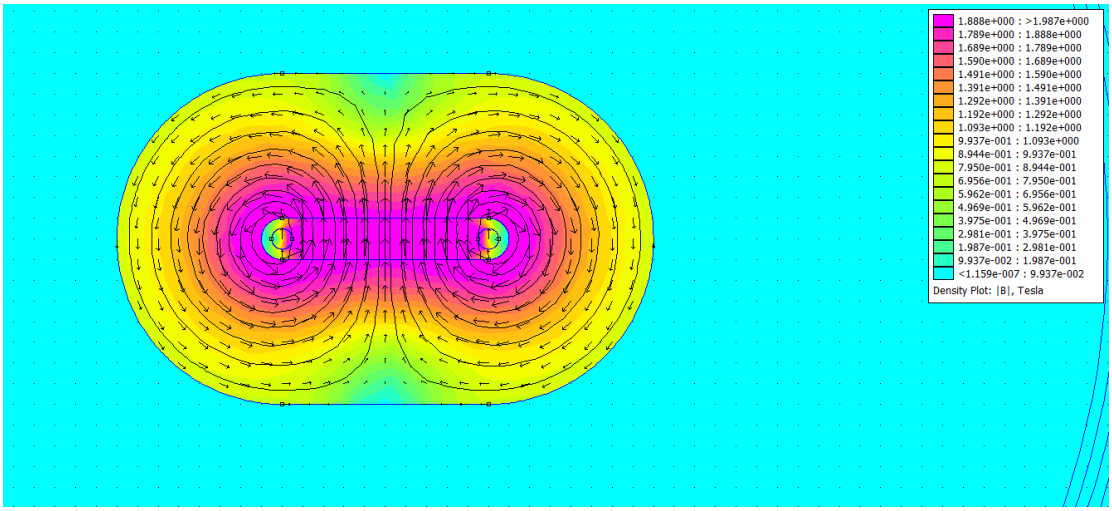

Figure 36: Magnetic Shell Setup (Average Flux Density Between Rails = 1.97T)

The greater flux densities mean that the K is multiplied by the same factor without increasing the resistance of the circuit. As an added benefit the magnetic shell itself can be used to reinforce the rails as well. However as illustrated above the multiplication factor degrades significantly if the shell saturates (purple regions of core). Much of the amplified flux pierces the rails leading to large increases in rail force. Due to saturation, the multiplication factor decreases and the effective air gap where the projectile sits widens as seen by the magnetic field. In other words, an increase in flux in saturated regions of the shell will behave as if that part of the shell is

a vacuum. Meaning, increasing the current beyond this operating point will yield an increase in flux identical to the no shell case. Furthermore, this design has the undesired effect of increasing the inductance of the entire system by the same multiplication factor that the flux increased by. This can be countered by having field windings around the shell that saturate it right before the railgun fires. That setup can be described as a railgun situated within an electromagnet that is energized first before the railgun is allowed to fire.

4.3 Projectile "Wrap Around" Design

One possible design is to use round rails and to drill two holes in the projectile with the same spacing as the rails such that the rails slide through the holes. Figure 33 shows what the cross section of such a design might look like with the bottom blue portion holding the rails in place at the base.

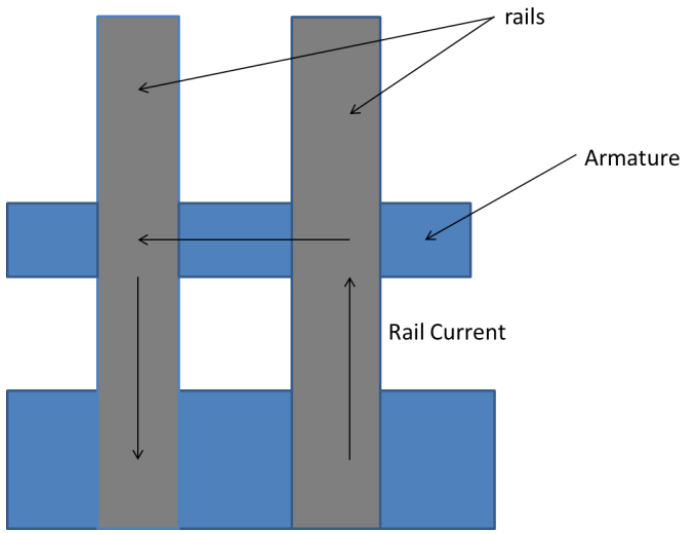

Figure 37: "Wrap Around" Projectile Design

By fitting the projectile over the rails as shown in Figure 33 the projectile can be thought of as wrapping around each rail. The advantage of this design is that as the rails push away from each other they push against the projectile ensuring the electrical contact remains stable. This also has the benefit of the projectile reinforcing the rails at the end of the "conducting length" (The section of rail that is conducting current). This is particularly desirable because the projectile is likely a block piece of metal that offers a high tensile strength naturally which is perfect for bracing

the rails with. In other words the projectile can likely withstand a lot of force from the rail before it deforms and stretches.

This design especially favors a magnetizable projectile as large fluxes can be induced within the projectile. In fact, with a magnetic projectile this design is similar to the magnetic shell railgun with the projectile itself acting as the magnetic shell without the airgap. However this design doesn't suffer from the excessive inductance added by the "shell" because the shell in this case only amplifies the flux density along the projectile and nowhere else. Since the airgap has been eliminated the factor of increase in flux (and K) generated is near μ_r if the core doesn't saturate. Another benefit is that the projectile keeps the flux mostly contained within itself and away from the rails so it actually can achieve a rail force significantly lower than all the other designs. In fact, if the outer edges of the projectile saturate the resulting fringe flux begins generating a Lorentz force that pushes the rails inward around the projectile's location on the rails. Below Figure 38 shows an FEMM simulation of a well-designed 1m long wrap around with 2" spacing between the rails and a projectile that is 1" thick around the rails at a rail current of 180A while Figure 39 shows the same setup but with a rail current of 5kA. It's worth noting that the standard rail design in this configuration only generates an average flux density over the projectile of about 3mT meaning in this particular instance we generate 700 times more force than the standard design which is little over 19N.

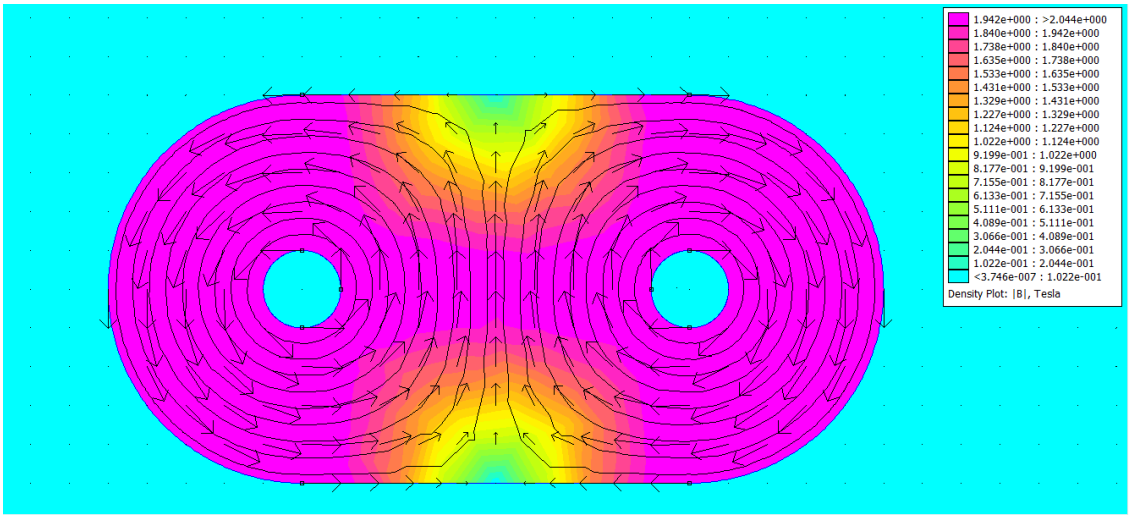

Figure 38: Well Designed Wrap Around (Average Flux Density = 2.1T)

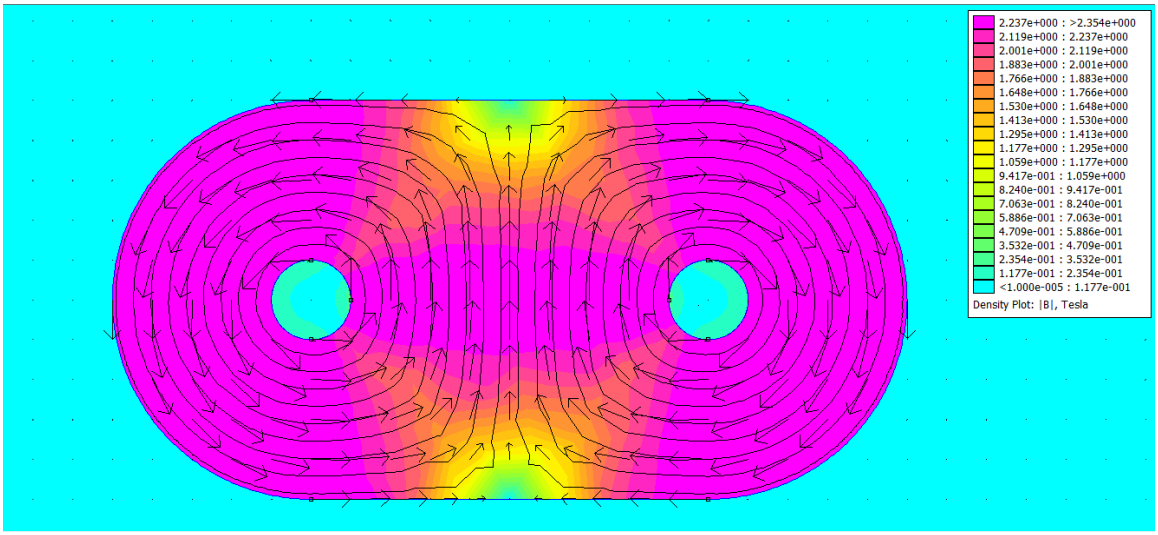

Figure 39: Saturated Projectile (Average Flux Density = 2.4T)

We can see in Figure 39 significant amounts of flux density are now permeating through rails shown as a green haze. Only the flux in the rails near the middle of the projectile would generate a Lorentz force that pushes the rails outward. The flux everywhere else is actually travelling in the opposite direction in the rail Figure 40 is larger picture of the right rail shown in Figure 39

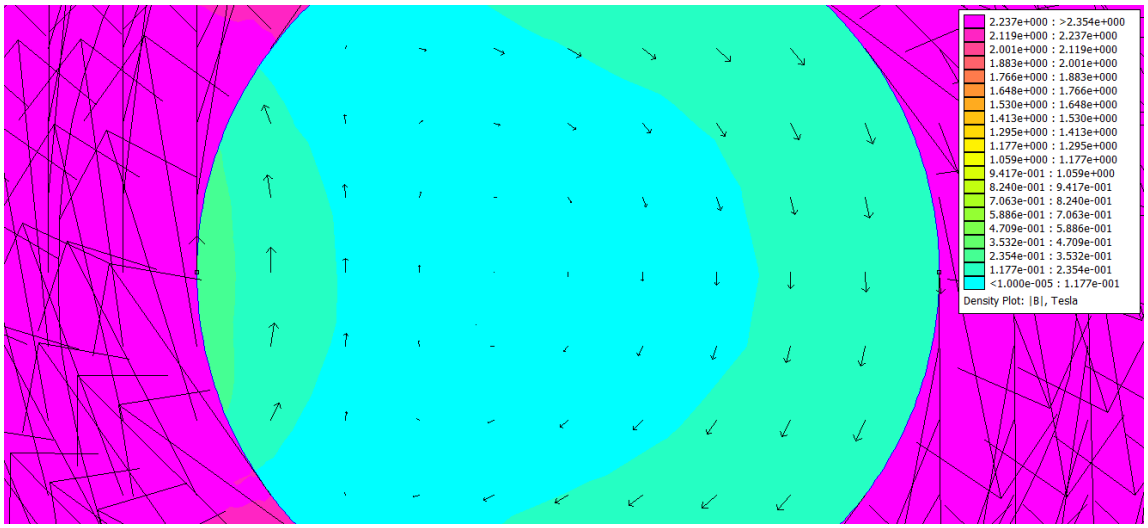

Figure 40: Fringe Flux in Right Rail

This flux that is travelling opposite of the flux in the middle of the projectile induces Lorentz force that is pushing the rails inward. In fact there is more flux travelling downward in Figure 40 than upward meaning that the rail is actually pushed toward the center of the projectile

as does the left rail was well. It's worth noting that this is only at the projectile's location and that outside of the projectile the railgun behaves identically to the standard rail design. The average flux density over the projectile only increased by 14% so any gains in projectile force are mostly through the fact that now more rail current is travelling through roughly the same B field. The saturation of the B field is what leads to the multiplication factor applied to the K of the system effectively dropping.

There are drawbacks associated with this design. Namely the fact that the projectile must have two holes drilled into it and must have a relatively high tensile strength to prevent the rail forces from warping the projectile itself. This design is really only good when using a magnetic projectile or armature that the application might prohibit. Below in Table 3 is a summary of the various tradeoffs between each design.

Table 3: Summary of Design Options

	High K Value	Low Inductance	Good Electrical Contact	Low Rail Force	Low Rail Current
Standard	No	Yes	No	Yes	No
Wrap Around	*Maybe	Yes	Yes	Yes	Yes
Augmented	Yes	No	No	No	Yes
Mag. Shell	Yes	No	Yes	Yes	Yes

*Yes if using a magnetic projectile, No otherwise

5 Testing

It should be noted that to ensure that L>>S when the projectile begins conducting current otherwise there won't be enough rail to generate the B field for the for the projectile's Lorentz force. This leads to little force being generated and much energy in the beginning being released as heat rather than projectile kinetic energy. For testing we selected the wrap-around design since that was the easiest to machine and ensured that good electrical contact was maintained between the projectile and rails as the system fired. As mentioned in section 4.3 this design works best with a magnetic projectile because it essential is the magnetic shell design with the projectile acting as the shell with a reduced rail force that is possibly forcing the rails inward around the projectile. As mentioned back in section 2.5, this design is a situation when L' is no longer linked to projectile force, and is due to the fact that most of the flux in the current loop formed by the rails and the projectile depends mainly on μ_0 while the projectile force depends on μ_r of the projectile. We chose to use approximately a 12" small scale model for ease of testing and safety concerns.

5.1 System Build

The initial test was completed to gauge how accurate our assumptions were regarding arcing and system resistance, and was designed to be cheap and easy as possible to machine. We chose aluminum as the rail material as it was relatively inexpensive and exhibits a similar resistivity to that of copper. The stand consisted of 1' long section of a wooden 4x4 post with two holes cut in one side to fix the rails in as shown in Figure 41.

Figure 41: Railgun Stand

Any extra holes that are seen on the wooden block were due to mistakes in the machining process due to the tolerances having to be as tight as possible. One mistake at any part would warrant doing it all over again. The thin piece of black metal bridging the gap between the aluminum rails is the iron projectile that was used in subsequent tests. Not shown in the picture above are the rails protruding out the bottom slightly where the power supply was to be connected to the rail system. There was also an aluminum projectile that was cut to geometrically resemble the iron projectile as close as possible. The rails were also electrically insulated near the wooden base to prevent the projectile conducting when at rest. To fit the insulation and the projectile over the rails the insulated part needed to be ground down and then insulated.

One of the hardest parts when building this setup was making a reliable and inexpensive firing system that we could use to safely fire the gun from a distance. We salvaged a solenoid off a piece of machinery that later was discovered could run off 120V DC or 240V DC for a short time. The goal was to have a pull string firing system that could safely be activated with the solenoid remotely. This was accomplished by drilling a small hole through, and tying one end of a small nylon rope to a small piece of wood that was situated on the edge of the block stand and underneath the projectile. When the rope was pulled the piece of wood would teeter on the edge of the block and lift the projectile up passed the insulated parts of the rails where the projectile would then conduct. The rope was then fed underneath the block (after adding “feet” to raise the

bottom off the ground) to where the solenoid would be sitting and tied to it as well. To ensure the solenoid stayed in place during firing it was fastened to another block of wood as seen in Figure 42 that was pushed up against the stand. The drill bit below was sometimes used to add additional space between the block and the solenoid as the nylon string proved to be a bit too long at times.

Figure 42: Firing Solenoid

The two wires seen in Figure 42 ran to a switch and a full wave rectifier that was connected to a transformer that stepped up the voltage as shown below in Figure 43.

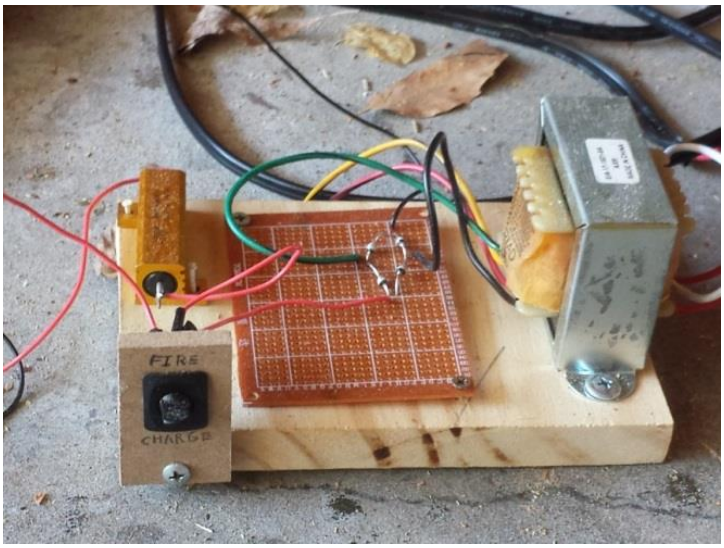

Figure 43: Transformer Circuit

This part of the setup contained all the necessary electronics to charge the capacitors and fire the railgun. The switch that can be seen above switched the output from the full wave rectifier to the charging circuit (CHARGE) or to the solenoid directly (FIRE). For clarity the circuit schematic is shown below in Figure 44.

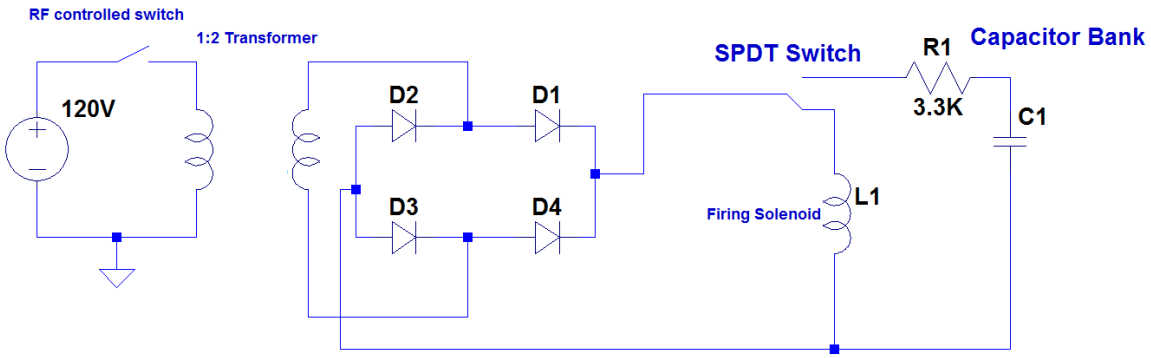

Figure 44: Transformer Circuit Schematic

The 3.3kΩ resistor was needed in the design to ensure there were no current spikes from the transformer at the beginning of the capacitor charging cycle that could damage the transformer or any of the other electrical components that made up the circuit. If the transformer were connected directly to the capacitor there would be little resistance to impede the current thus leading to surge currents at least in the beginning. As the capacitor charges the voltage drop over tiny resistance would decrease as would the current. The rectifier and resistor could also be used to discharge the capacitors in the case of a misfire by switching the leads. Not shown in any of the pictures is the RF controlled switch. The RF switch was a small power strip that could be wirelessly turned on or off at an approximate distance of 10 feet with a remote. The switch was intended to be the final trigger that would fire the railgun. The idea being that the capacitors were already charged and, with the RF switch cutting the power to the whole setup, the switch would be flipped to “FIRE”. As soon as the RF switch closed and restored power to the transformer the transformer would energize the firing solenoid and fire. After firing, the power had to turned off soon as possible as the solenoid wasn’t really designed to be wired to 240V and would likely burn up if left on for too long.

We were provided with 4 Cornell Dubilier 2.5mF 360V capacitors as shown below in Figure 45 for power storage.

Figure 45: 7P252V360N082 Capacitors Utilized in Setup

Considering the budget for this project it was decided that these capacitors were the best ones to use initially despite the fact there are much better and expensive capacitor banks available for purchase. The data sheet stated their maximum ESR to be 80mΩ. It was thought that would make up the bulk of the system resistance for this setup [12]. A tabulation of the physical dimension of the gun is shown below in Table 4.

Table 4: Characteristics of Railgun

Rail Length	9”
Rail Width	.25’
Space Between Rails	1’
Max Rail Resistance	.383mΩ

5.2 Test #1

This test was conducted before we had completely determined most of the previous expressions and built the simulator. We needed to see how well our assumptions about various parts of the project such as the arcing and static resistance held up. We tested both 4 gram aluminum and 12

gram iron projectiles at 100V and 200V with a single charged capacitor. Figure 46 shows the setup for the aluminum test.

Figure 46: Aluminum Projectile Test Setup

Figure 47: 200V Aluminum Projectile Test Fire

Figure 48: Capacitor Voltage (Yellow Line) Over Time

Figure 47 above shows the 200V aluminum test mid fire. While it's an impressive display "sparks and sound" it did little to lift the projectile through the rails. The iron projectile tests yielded

similar results as well. These results as the oscilloscope reading (shown in Figure 48) of the capacitors indicated that the peak currents were as high 12.5kA. Observing the discharge curve reveals that electrical contact between the rails and projectile remained steady throughout the discharge. Readings indicated that the system resistance was 15.4mΩ, drastically different then the approximately 80mΩ we were expecting. It's worth noting that both capacitors stopped discharging at about 30V when by all appearances they should've discharged completely.

Later when we completed the simulator, we simulated our design to see just why it failed to accelerate the projectile up the rails. The results are shown below in Figure 49 & Figure 50, and while the current pulse was 12.5kA its duration was still far too short for the projectile to gain any speed. In the end the aluminum projectile was simulated with our gun's physical dimensions, zero initial velocity, and R_{sys} of 15.4mΩ to not even reach a height of .5mm.

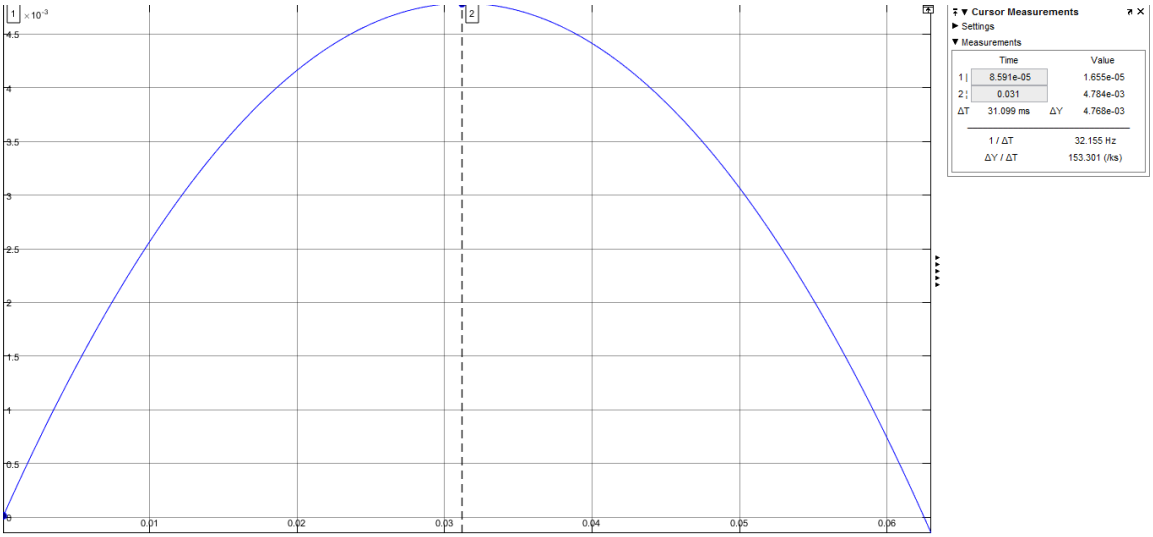

Figure 49: 200V Aluminum Test (.5mm max)

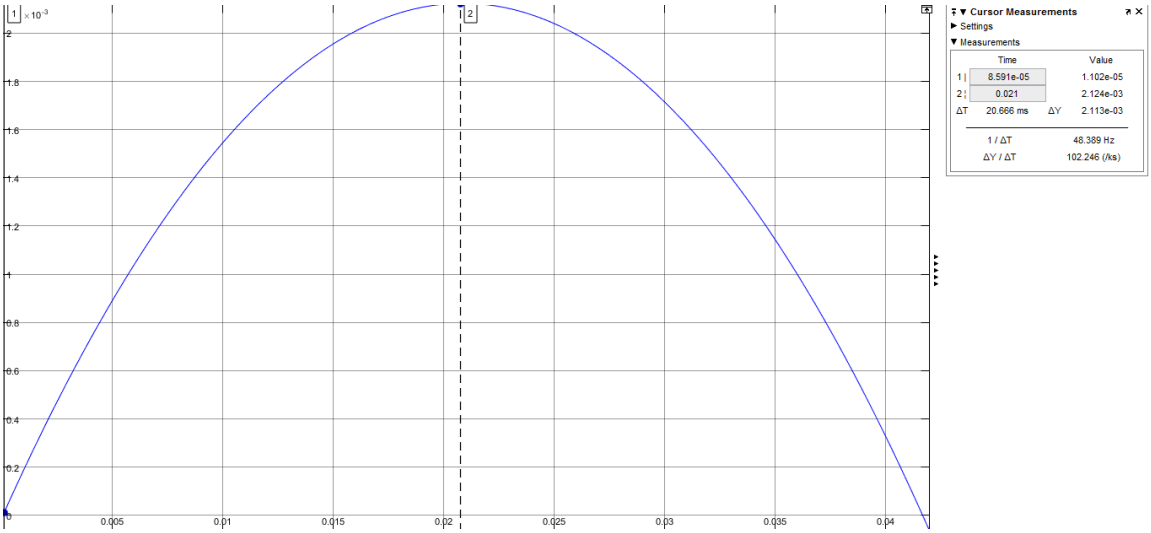

Figure 50: 200V Iron Test (2mm max, core gain = 2)

The iron projectile was harder to simulate properly due to the saturation of the internal B field of the projectile with such high rail currents. It required the use of FEMM [13] as well as the simulator we made. Even considering the best case scenario (core gain = 2) the iron projectile would only make it about 2mm up the rail before falling back down. The iron projectile's failure was due to the same reason why the aluminum projectile failed.

5.3 Assessment of Rail Endurance

Another aspect that these tests were supposed to determine was just how well the rails held up during the tests. Shown below in Figure 51 is what the aluminum rails looked like after the tests which at one point sourced 17.5kA.

Figure 51: Erosion of Rails After Test #1 (17.5KA for approximately 35μs)

We didn't choose aluminum as a rail material because it was strong but it became clear that if anyone was going to do larger scale designs they're going to need much harder material with a higher melting point for the rails. Right then we decided to use copper tungsten rails as tungsten has a very high melting point and is far less likely to be vaporized by the arcing. The copper mixed in the alloy helps the tungsten conduct better than regular tungsten at the cost of compromising corrosion resistance just a little bit [16]. Due to this modification the resistance of the rails nearly doubled.

5.4 Test #2

Eventually we had acquired a 3000F super capacitor that according to the data sheet had only .29mΩ of ESR [17]. The main limitation with this capacitor was its 2.7V rating. This made it very susceptible to resistances in the system. However, despite this it still could supply over 9kA of current initially and would have a current pulse that was much longer. We simulated the aluminum projectile under these conditions (R_{sys} = 1mΩ) and found favorable results in Figure 52 below.

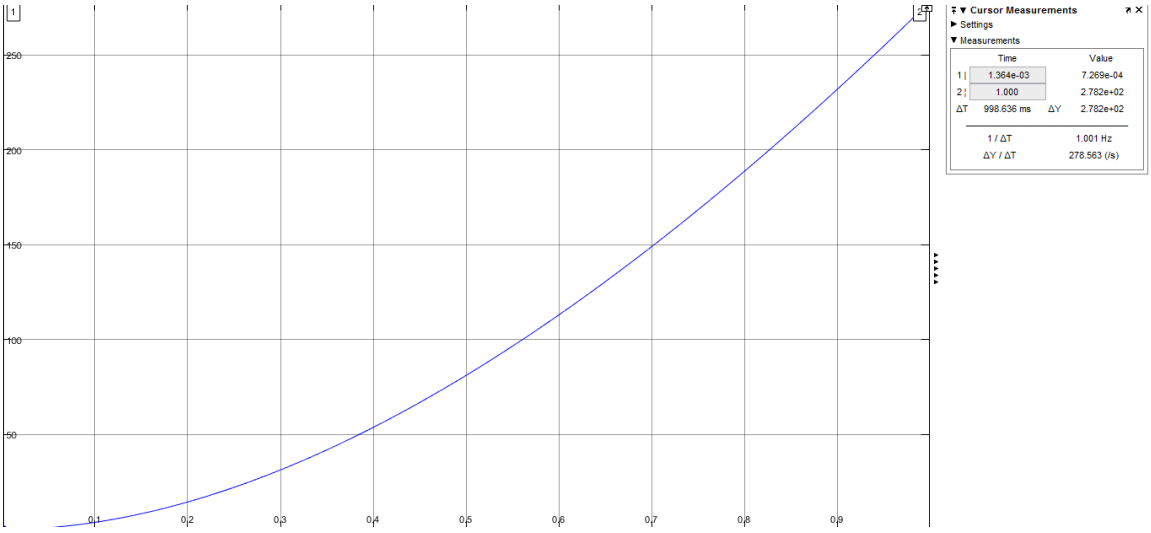

Figure 52: Aluminum Projectile Position Simulation

Simulation showed the projectile would clear the rails easily. The iron projectile would fair even better since the current pulse would be at least a 100 times longer and saturation effects wouldn't be as problematic since the peak current was approximately 9kA.

However, the terminals of these capacitors ending up being far more problematic as they were "stud-weld" terminal type. We were supposed to weld studs to the capacitor terminals with a stud welder that we did not have nor did we have the stud that would allow us to fasten wire to the terminals of the capacitor. We couldn't use any other device because the heat would've likely destroyed the capacitor. We improvised by pinching the wires against the terminals of the capacitor by clamping pieces of aluminum over the wires. This was not ideal since the terminal stubs only allowed us to press the wire to the terminals which typically makes poor electrical contact.

The current charging circuit wasn't going to be enough either as it would take nearly 31 hours to charge a capacitor that large. We were lent a variac (variable transformer) and acquired two full wave rectifiers. We put the rectifiers in parallel (to source more current), hooked their output to the capacitor, and carefully dialed the voltage up using the variac and an ammeter to monitor the current. This allowed us a current source of about 5A which would charge the capacitor in little less than half an hour which we determined to be sufficient.

Due to the long charge times we only ran this test once with the iron projectile with the result shown below in Figure 53.

Figure 53: Result of Test

The iron projectile moved crookedly up the rail and got stuck. The other problem was the capacitor only discharged to about 2.3V despite the projectile still making contact with the rails. Later when we looked at the video shot on a phone with a frame rate of 400fps and noticed some very faint smoke rising from one of the terminals and then stopping. This likely was due to poor contact from a wire that wasn't fully against the terminal. We had to fix these problems and retest before we were going to draw conclusions from the results about the design itself.

5.5 Test #3

For test #3 we decided to use a differently shaped projectile shown in Figure 54 that resisted binding and getting stuck along the length of the rails. The measured near the rails the projectile was .75" thick, .5" thick in the middle, and was .5" wide.

Figure 54: Improved Projectile

This covered a longer section of the rail at any given time which led to less of a chance that it would get stuck. This would hopefully rule out friction as the cause of the projectile not launching through the rails. The disadvantage of this projectile was that it was significantly heavier than the previous projectile weighing in at 50g. This would result in lower velocities but according to the simulation results shown below in Figure 55 we would still see the projectile clear the rails.

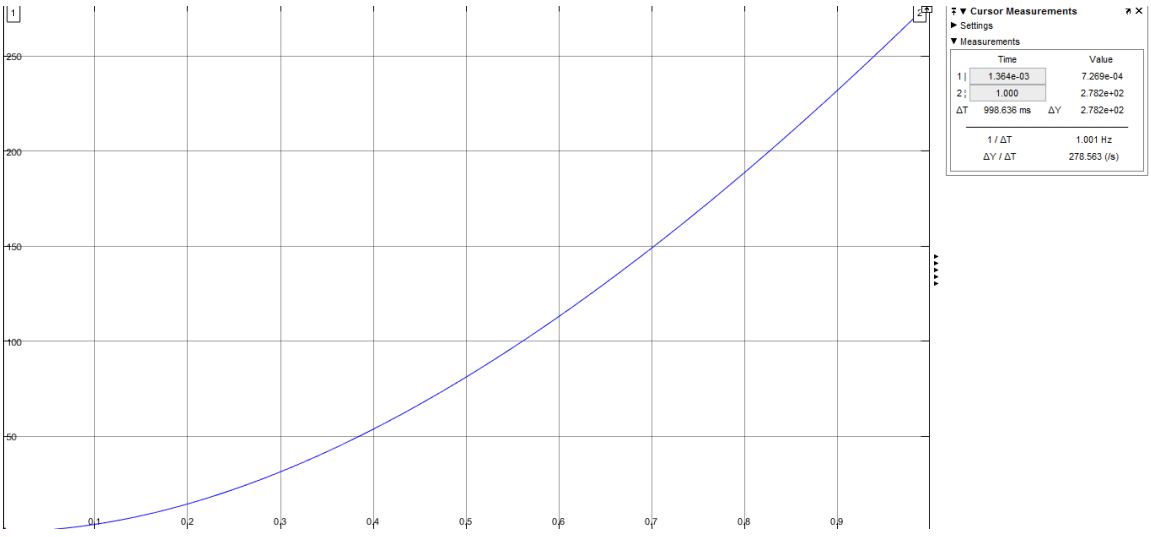

Figure 55: Simulation Results For Improved Projectile (Core Gain = 2)

The setup had to be modified to accommodate the new projectile's geometry as it 5/8" taller on the rails. The insulation was extended, the other side's insulation removed, and a wedge shaped piece of wood that the help firing system to grab the projectile better as shown below in Figure 56. This led to better, more consistent firing and easier sliding for the projectile. Also holes were drilled into the aluminum plates allowing them to fit more snug on the terminals of the capacitor. This lead to a far more secure connection for the wires and it allowed us to clamp down harder and more of the wire against the side of the terminal.

Figure 56: Modified Setup

The results were equally disappointing as the capacitor again barely discharged through the projectile. Evidence suggests the copper and aluminum contacts oxidized at that moment thereby preventing any more current from flowing. Later we tried shorting the fully charged capacitor with just a piece of copper wire and found that while the initial reaction was violent it would soon stop sparking and even cool down. We had to repeatedly rub the wire against both terminals to sustain that initial reaction and after a while as the capacitor discharged even that would fail too. **Low voltage – high current power supplies may be viable for a railgun, but much care must be taken to avoid any oxide layers from impeding the flow of current.** This can be done if all the connectors along the current path are welded or fused together. That way if

any oxide forms, it will be on the outside of the metal and not in the way of the current rushing through.

5.6 Test #4

With tungsten copper rails we decided to power the system with the 360V capacitors as the voltage was high enough to puncture through oxide on any of the metal. We also wanted to see how the rails held up under repeated tests. This time we decided to put 4 of the 2.5mF Dubilier Capacitors used earlier in parallel and continued to use the improved projectile as the additional weight was worth it if it eliminated the metal binding issue. We assumed that the majority of the system resistance was due to the capacitors still. Therefore 4 capacitors in parallel should've divided the system resistance by roughly 4. We then simulated the entire setup as described above and were given the results shown below in Figure 57.

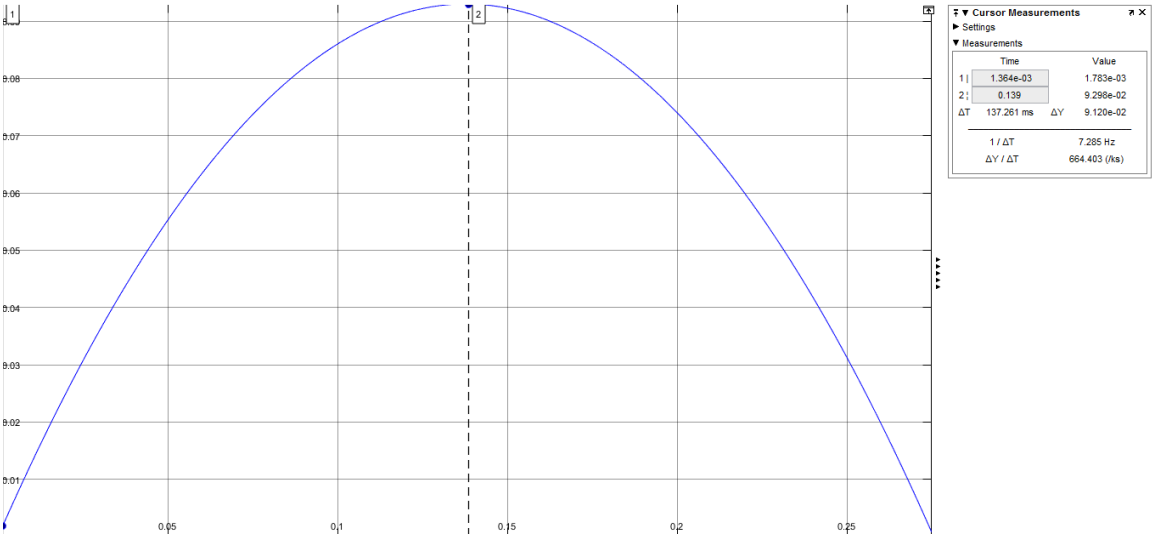

Figure 57: Results For Improved Projectile (9.3 cm max, Core Gain = 2)

We decided to help the projectile's magnetization along by properly orienting, and sticking on both sides, two neodymium magnets. This would ensure that the B field at the very beginning is already at ~1.4T and hopefully would give us results we could see. We performed a 100V, 200V, and a 270V (shown in Figure 59) test that both ended with the projectile hardly moving, and one of the wires breaking free from a terminal within the capacitor bank. An interesting fact that we

missed but later caught on video was the wires that ran to the railgun move apart from each other during the firing which can be seen by comparing Figure 58 and Figure 59.

Figure 58: Setup With Wires At Rest

Figure 59: Wires Separating During Firing

The reason the wires did this is the same reason why the rails experience a force that repels them apart. Even though current pulse is very brief, it's very intense and is running in the opposite direction of the current in the opposing wire. This creates a force large enough to accelerate the wires away from each other in that brief firing period.

The damage inflicted on the copper tungsten was simply the oxide being blown off the surface of the rails as shown in Figure 60.

Figure 60: Minimal Damage Done to Copper Tungsten Rails

Again the capacitors stopped discharging once they've reached 30V shown in Figure 61. By now it was clear that there is some barrier preventing the capacitors from discharging below 30V.

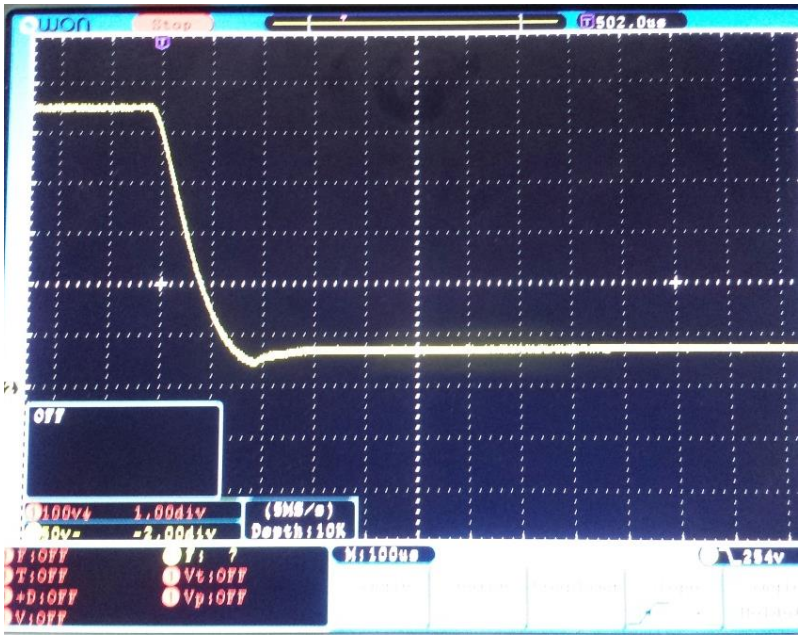

Figure 61: 270V Discharge Curve

Treating the circuit as a purely RC circuit we estimated the system resistance to be about 11mΩ this time. This showed that our assumption about the system resistance being dominated by the ESR of the capacitors to be false. If it were true the system resistance should've been around 4mΩ or a fourth of the original system resistance. This was likely due to the connectors we were using to fasten the wires from the capacitor bank to the rails and the wires themselves. We were limited to about 12" of 12 gauge wiring (contributing about 2mΩ to the system resistance) as the terminals of the capacitors were very close to each other. If the wire were any larger we would run the risk of an arc forming across the terminals where the wires were fastened. To compensate we attempted to use the shortest lengths of wire that were manageable, but ultimately it likely contributed a few milliohms of resistance to the total. Table 5 below is a summary of all of the experimental results of all the tests.

Table 5: Summary of Experimental Results

	Projectile	Trial #1	Trail #2	Trial #3
Test #1	Aluminum	100V -> 37V	200V -> 35V	270V -> 31V
	Iron	100V -> 38V	200V -> 34V	X
*Test #2	Iron	2.7V ->2.3V	X	X
Test #3	Improved Iron	2.7V -> 2.6V	X	X
Test #4	Improved Iron	100V -> 34V	200V -> 33V	270V -> 28V

*Aluminum rails switched out for 12" long, .25" in diameter copper-tungsten rails for subsequent tests including this one (~ twice the resistance of the aluminum rails)

5.7 Frequency Response of Projectile

There is another aspect that was neglected in this analysis but is important nonetheless and that is the AC response of the material's B-field. Since the projectile is a solid that is conductive to electricity it tends to form currents that cancel out parts of the time varying internal B-field in the projectile [9]. This is particularly detrimental because the internal B-field is what determines the strength of the projectile force, and the rate of change for the B-field large (on the order of MT/s possibly GT/s) in this device. Figure 62 and Figure 63 shows the difference between DC currents and static B-fields from time varying ones simulated in FEMM respectively.

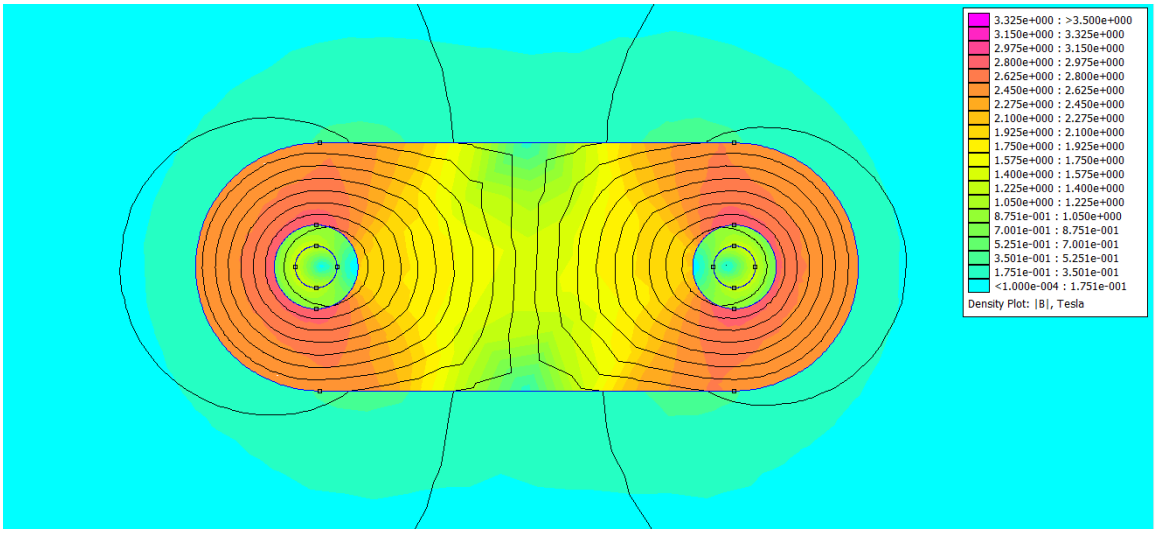

Figure 62: B-field at Static Current

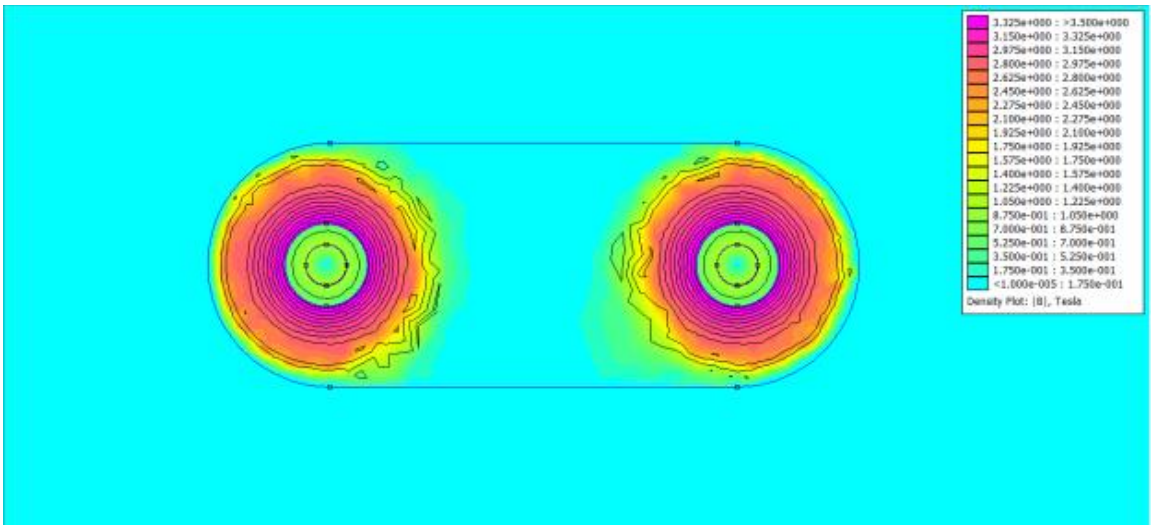

Figure 63: B-field With Time Varying Current (1KHz)

We can see that the B field is a bit more concentrated in the areas around the rail but it fails to make up for the loss of the B field between the rails. Since most discharge times for practical railguns tend to be at least in the millisecond to microsecond range this means much of the frequency content of the signal probably lies near 1KHz and beyond. To see this note the Fourier Transforms of the following functions:

$$u(t)e^{-\alpha t} \rightarrow \frac{1}{\alpha + j\omega}$$ Equation 60

$$A * rect\left(\frac{t}{\tau} - \frac{\tau}{2}\right) \rightarrow A\tau * sinc\left(\frac{\omega\tau}{2\pi}\right) e^{-j\tau/2} \quad \text{Equation 61}$$

Where α represents the time constant of the RC equivalent circuit and τ represents the duration of a rectangular pulse created by a pulse forming network. In both cases if the discharge time is less than 1ms a significant portion of the frequency content lies beyond 1kHz. This is detrimental for Figure 63 since that leads to even more loss of the B-field along the distance between the rails and force on the projectile. The only realistic way to fight this kind of phenomenon is to use a laminated projectile. In other words, the projectile must be formed by stacking electrically insulated pieces of metal next to each other to minimize eddy currents that weaken the internal B-field. With the laminations oriented parallel to the B field of the rails, the laminations acts as barriers to eddy currents that typically travel perpendicular to the changing B-field. However, the laminations are still perfectly capable of conducting current through the sides of the projectile parallel to the laminations. Figure 64 illustrates the setup.

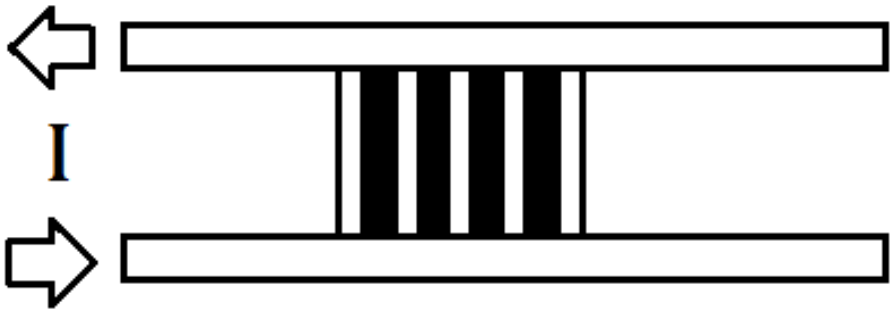

Figure 64: Laminated Projectile Conceptual Drawing

However this will increase the resistance the projectile and likely sacrifices the structural integrity as the lamination material is likely weaker than the metal it's replacing. Ultimately the projectile's conductive nature responsible for propelling the projectile down the rails is also slowing it down with the eddy currents that accompany such an intense change in the B field of a material.

6 Conclusion

We have successfully derived and utilized useful equations that can find the rail force and one that can compute the total performance of a capacitor railgun given capacitor bank specs, physical railgun specs, and the projectile initial velocity. Through FEMM software we were able to observe the different B fields generated by varying rail geometry, and discover how and why cylindrical rails offer superior B field strength. While deriving many of the equations, we developed a very useful equivalent model and way of thinking about the railgun, strengthening our intuition about how the system behaves under different conditions. We now have a simulator that can approximate projectile velocity solutions and plot various railgun parameters such as back EMF and rail forces over time. We examined different designs and showed in at least one of them that it's possible to eliminate or reverse the force exerted on the rails around the projectile's location on the rails during firing. During testing we proved copper-tungsten rails are a viable solution to the rail endurance problem present in most designs. Finally we demonstrated the underlying problem with using conductive projectiles in railguns and offered a solution to limit eddy currents generated by the changing B field present in the railgun.

There is still more testing that must be done on this system before any final conclusions can be drawn. One of the major factors that were ignored because of the difficulty of the calculation was friction. Potentially it can be enormous as the rail force is the main component of the normal force that pushes the rails against the projectile. At the same time the rails are anchored in the base and therefore the beams must first deflect far enough to contact the edges of the projectile before the rail force begins contributing to the rail normal force and thereby the frictional force. Ideally the force to deflect the rails far enough for friction to be a problem would be as large as possible. However, as the projectile travels further down the rails and assuming constant force exerted along the section of rail that the projectile has covered, this deflection increases roughly proportionally to the distance travelled by the projectile as shown in Figure 65. In reality the angle of deflection in each rail would also increase as the force is being applied further and further down the rail as well as along the length of the rail. This makes it especially difficult to brace the rails in such a way that minimizes the force pushing the rail into the projectile.

Considering all of this leaves much to be discussed before any conclusions, positive or negative, can be made seriously.

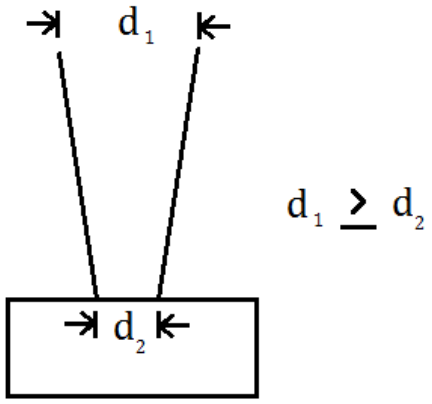

Figure 65: Approximate Rail Deflection Pattern

The other issue was the search for a suitable power supply. Due to the fact that system resistance was the number one way to improve system performance we chose the lowest possible ESR power source that we could find – capacitors. Capacitors are great for their simplicity and large power output due to their typically low ESR. When combined in parallel they can effectively form a larger capacitor with an even lower effective series resistance. However care must be taken to ensure that the capacitor voltage is large enough to form an arc between any air gap present between the rail and projectile, and puncture the oxide on both metal surfaces. This was evident by the fact that in both high voltage tests the capacitors discharged to around 30V before stopping. The arc itself is usually considered by many to be near superconductive as often the only limiting factor for the current traveling through the arc is the max current that can be supplied by the power source [14]. If the oxide isn't punctured, a stable arc tends to not form leading to much higher system resistance and weaker discharges.

However capacitors by themselves have undesired effect of creating large spikes of current when discharged rather than the preferred rectangular pulses. This has the negative effect of creating potentially large eddy currents that will counter the B field within the projectile and reduce projectile force. This is suspected in all designs and a novel projectile such as a

laminated projectile has a good chance of reducing such currents. Alternatively one can use pulse forming networks [15] to ensure that much of the frequency content of the current pulse is contained in the lowest frequencies possible. This has the benefit of avoiding very quick changing B-fields and therefore reduces losses through eddy currents by sacrificing a quick discharge time and possibly low system resistance.

Pulse forming networks were avoided altogether because they often add hundreds of milliohms to the system resistance and we were trying to minimize that as much as we could [15]. They also tend to increase the circuit's inductance and large reverse voltages following the discharge period must be contended with. This can be particularly dangerous if electrolytic capacitors are being utilized as a large reverse voltage can puncture the insulation on a capacitor electrode, causing an internal short, and sometimes an explosion. Ultimately achieving an R_{sys} of 11mΩ was not enough and was likely due to the mechanical connectors that fastened the wires from the capacitor bank to the rails themselves. We were forced to use the same mechanical connectors as we later transitioned to copper tungsten rails and were unable to weld or otherwise fuse the wires in some way to the rails. Ideally all connections should be made through a metallic bond of some kind. This ensures that there are no oxide layers that form in the current path and yields the lowest ESR of any electrical connection. In our setup and all likelihood a layer of oxide formed between the connector and rails which potentially increased the system resistance by a substantial amount.

7 Future Work

A larger scale model is needed to properly measure phenomenon like friction and rail deflection. We recommend that if this is undertaken, that the testers have some means to accelerate the projectile as fast as possible before it conducts across the rails. This will ensure that any differences in initial and final velocities can be measured and, as stated in Equation 55, the machine runs more efficiently overall with high projectile initial velocity. However, care must be taken as the back EMF of the machine increases as the rail current increases and the projectile velocity increases. The only way to maintain high power output in this case is using higher voltage power supplies that can maintain the necessary currents at higher voltages. This favors capacitors as they can be charged to extremely high voltages before discharging and by extension can maintain high power output even in the presence of high back EMF. However as mentioned before this potentially will introduce enormous losses through eddy currents in the projectile. Therefore the application must be considered first before anything else as some metrics are likely going to be sacrificed to meet other specs.

BIBLIOGRAPHY

[1] "Navy Evaluating Second Electromagnetic Railgun Innovative Naval Prototype." *Office of Naval Research Science and Technology*. Office of Naval Research, 9 Oct. 2012. Web. 1 May 2016.

[2] "Electromagnetic Railgun." *Office of Naval Research Science and Technology*. Office of Naval Research. Web. 13 May 2016.

[3] Villeplee, Fauchon. "Patent US1421435 - Fauchon-villeplee." *Google Patents*. Web. 1 May 2016.

[4] Iskander, Magdy F. *Electromagnetic Fields and Waves*. 2nd ed. Long Grove: Waveland, 2013. Print.

[5] "Right-hand Rule." *Wikipedia*. Wikimedia Foundation, 2 May 2016. Web. 1 May 2016.

[6] Johk, Carl T. A. *Engineering Electromagnetic Fields and Waves*. 2nd ed. New York: Wiley and Sons, 1988. Print.

[7] "Chapter 9 Sources of Magnetic Fields - MIT." *Web.MIT.edu*. MIT. Web. 23 Feb. 2016.

[8] Hayt, William H., Jr., Jack E. Kemmerly, and Steven M. Durbin. *Engineering Circuit Analysis*. 8th ed. New York: McGraw-Hill, 2012. Print.

[9] DeMaw, M. F. Doug. *Ferromagnetic-Core Design Application & Handbook*. Englewood Cliffs: Prentice-Hall, 1981. Print.

[10] Jeffrey Joseph Maniglia Jr. *DESIGN, FABRICATION, AND TESTING OF AN EMR GUN BASED ORBITAL DEBRIS IMPACT TESTING PLATFORM.* California Polytechnic State University, San Luis Obispo

[11] Michael R. Lockwood. *DESIGN AND CONSTRUCTION OF AN EXPANDABLE SERIES TRANS-AUGMENTED ELECTROMAGNETIC RAILGUN.* Naval Post Graduate School Monterey, CA.

[12] N.p., n.d. Web. 5 May 2016. http://www.alldatasheet.com/datasheet-pdf/pdf/240415/CDE/7P252V360N082.html

[13] N.p., 6 Apr. 2014. Web. 9 Mar. 2016. http://www.femm.info/wiki/HomePage

[14] Ayrton, Hertha Marks. *The Electric Arc*. London: "The Electrician" Printing and Pub., Limited, 1902. Print.

[15] "Pulse Forming Networks." *General Atomics & Affiliated Companies*. N.p., n.d. Web. 1 Mar. 2016.

[16] "Copper Tungsten." *Torrey Hills*. N.p., n.d. Web. 2 Feb. 2016. <http://www.torreyhillstech.com/cuwdata.html>.

[17] "K2 2.7V Series." *Maxwell Technologies*. N.p., n.d. Web. 13 Mar. 2016.

APPENDIX: Table of Variables

Name	Variable	Units
Distance Between Rails	s	m
Conducting Length of Rail	L	m
Permeability of Vacuum	μ_0	H/m
Rail Width	w	m
Rail Current	I	A
Rail Force	F_r	N
Projectile Force	F	N
Projectile Flux Gain	K	H/m
Inductance Gradient	L’	H/m
Projectile Velocity	v	m/s
Back-EMF	E	V
Source Voltage	V_s	V
Static System Resistance	R_{sys}	Ω
Instantaneous Efficiency	η	none
Stored Capacitor Energy	E_c	J
Initial Projectile Velocity	v_0	m/s
Final Projectile Velocity	v_f	m/s
Initial Capacitor Voltage	v_c	V
Voltage Over Resistor	v_R	V
Voltage Over Inductor	v_L	V
Rail Inductance	L	H
Distance Between Rail Endpoints	d_1	m
Distance Between Rail Basepoints	d_2	m